International Journal of Energy and Environmental Engineering
https://doi.org/10.1007/s40095-021-00399-9

ORIGINAL RESEARCH

Optimal power point tracking of solar and wind energy in a hybrid wind solar energy system

G. B. Arjun Kumar[1] · Shivashankar[1]

Received: 12 March 2021 / Accepted: 31 May 2021

Abstract

In recent years, Hybrid Wind-Solar Energy Systems (HWSES) comprised of Photovoltaic (PV) and wind turbines have been utilized to reduce the intermittent issue of renewable energy generation units. The proposed research work provides optimized modeling and control strategies for a grid-connected HWSES. To enhance the efficiency of the maximum power tracking of a grid-connected wind-driven Doubly Fed Induction Generator (DFIG) integrated with solar Photovoltaic (PV) system, connected to the DC link of the back-to-back converters of the Hybrid Wind-Solar Energy System (HWSES). Stator Flux-Oriented control is utilized to regulate the Grid Side Converter and Rotor Side Converter. The main objective of this paper is to apply the Maximum Power Point Tracking (MPPT) strategy to wind and solar PV systems to maximize the power extraction and to provide better integration of the hybrid systems into the electrical grids. Perturb and Observe (P&O) and Incremental Conductance (IC) MPPT algorithms are implemented to the solar PV system with varying solar insolation and their performances and efficiencies are compared. For varying wind speeds, Tip Speed Ratio (TSR) and Optimal Torque (OT) MPPT algorithms are implemented and their performances and efficiencies are compared for the hybrid system considering and integrating solar PV system. The optimal torque MPPT algorithm shows better responses when compared to the TSR method. A 2MW simulation model of the HWSES is developed and its performance is analyzed using MATLAB/Simulink environment. The implemented schemes have the advantage of tracking the optimal power output of the HWSES rapidly and precisely. Additionally, the provided schemes effectively control the power flowing through the HWSES and the utility grid, resulting in a quick transient response and enhanced stability performance.

Keywords Doubly fed induction generator · Photovoltaics · MPPT · P&O · Incremental conductance · Tip speed ratio · Optimal torque

Introduction

Renewable energies are certain to play a significant role in power generation in the future, due to the fast exhaustion of traditional energy sources. Wind and solar energy are the two main alternative energy sources that have the ability to alleviate some of the energy crisis. Nevertheless, independent investigation of such sources reveals that they are not entirely reliable due to their unpredictable existence [1]. Although, their utilization of hybrid energy schemes appears to be a more efficient and cost-effective approach in stand-alone implementations in remote locations where grid expansion is difficult. In [2] describes a new strategy for evaluating the effect of excessive allocation of renewable-energy-source (RES) integration on the operation of national power systems. Particularly, the approach begins with a review of the variance of RES development over ten years. Additionally, various simulation scenarios are described in terms of fluctuating wind power shares. In [3] a comprehensive analysis of recent advances in the sector of real-time energy management algorithms for hybrid RES and numerous approaches to real-time probabilistic power management is discussed both conceptually and empirically. The goal of this study was to establish models for the optimal design of the integration of renewable energy systems to meet energy needs [4].

✉ G. B. Arjun Kumar
arjungb@gmail.com

Shivashankar
chenduss123@gmail.com

[1] Department of Electronics & Communication Engineering, Sri Venkateshwara College of Engineering, VTU, Bengaluru 562157, Karnataka, India

Published online: 24 June 2021

There are many factors that establish wind formation. Winds are basically formed due to differences in the pressure on the earth's surface due to its irregularities and the rotation of the earth. This clearly indicates that wind energy directly depends on solar energy. Studies also indicate that solar energy and wind energy compliments and the extraction of both the energies in a particular area is moderate to high. Thus utilizing this concept, solar energy (i.e., solar Photovoltaic energy) is embedded in the wind energy conversion system to produce a hybrid solar-wind energy system (HWSES). Thus, a HWSES is essentially used in all the sectors replacing the traditional renewable sources. This combination of energy resources helps to reduce the carbon footprint on the environment, increases land utilization and also helps in integrating and utilizing the electrical power [5, 6]

Hybrid energy systems are a relatively powerful technology. It is anticipated that innovation will be able to develop in the future, allowing for greater applicability and cost reduction. There would be a significant level of optimization in design, making it easier to choose a model that is well suitable for specific applications [7]. There will be an enhancement in the level of communication between the modules. This enables more effective monitoring, control and diagnosis. Ultimately, the utilization of power electronic converters will increase Power electronic equipment is now being utilized in a large number of hybrid systems and their utilization is anticipated to increase as costs decrease and reliability enhances [8].

Wind energy and solar energy are the most reliable and fastest-growing distributed renewable energy sources. International renewable energy agency (IRENA) reports in 2020 states that the total renewable energy generation capacity amounts to 2537GW (where hydropower accounts for the largest share of 1190 GW). Wind and solar energy capacities are at 623GW and 586GW respectively [9].

In India, as of Feb 29, 2020, the total wind capacity installed was 37.7 GW, which is also the fourth largest wind capacity in the world. Also, the country's solar installed capacity was 35.73 GW as of June 30, 2020. India has set an ambitious target to reach 175GW of installed capacity from solar and wind energy by the year 2022, of which, 75GW of wind capacity and 100 GW of solar capacity [10, 11]. Solar and wind power generation which are variable in nature pore challenges to the grid and its stability. Many studies reveal that solar and wind energy sources are complementary to each other and have high to moderate power generation potentials. The hybridization of these technologies would help to maximize grid stability. Hence Ministry of New and Renewable Energy (MNRE) has issued a National wind-solar hybrid policy. This policy offers guidelines on supporting large-scale wind/solar/PV hybrid systems connected to the grid [12].

This initiative from the government of India has triggered the enlargement HWSES. There is extensive research involved toward the integration of the solar PV arrangement in WECS. The selection of wind turbines is a major factor involved in exploiting the output power extracted. Power generated from the wind turbine has to be of a fixed frequency. Hence, earlier fixed speed wind turbines were used to generate the power, which was operated at synchronous speed, limiting its wind energy capture range for only a fixed speed.

However, whenever there was a gust, that would pose heavy mechanical stress on the turbine and the conversion efficiency was very low as the power extraction from the wind took place for a rated speed, rejecting other speeds. With the advent of semiconductor technology and converters, the power of a constant frequency is obtained from varying speeds. This led to the evolution of variable-speed wind turbines. VSWT has a wide range of wind power capture due to its ability to extract power from sub synchronous and super synchronous modes. Thus, improving efficiency and achieve greater power quality. In addition, a wind turbine with variable speed control decreases the load stress on the turbine, blades and other mechanical structures [13, 14]. This results in a longer lifetime, improved power quality and higher efficiency. Doubly Fed Induction Generators (DFIGs) is the utmost frequently utilized adjustable speed wind turbine for a commercial generation. As the dynamic model of the DFIG relies on the nonlinear variables like stator and rotor currents, electromagnetic torque and stator and rotor flux is better than the FSWT. DFIG rotor is linked to the grid with the help of a back-to-back ($\mathfrak{b}t\mathfrak{b}$) converter, which allows only a fraction of the total system power, reducing the cost and the losses in the power electronic converter components. DFIG based WECS has a great capability to regulate the rotor speed in order to seek the maximum turbine power and with maximum power point tracking (MPPT) becomes the most sought-to-be wind turbine for commercial WECS installations [15, 16].

The following are the major contributions of the proposed HWSES.

- A comprehensive adaptive performance assessment of grid-connected or stand-alone HWSES is implemented by utilizing a DFIG and Solar PV System
- To reduce the dependency for the grid power for the rotor with the integration of the solar PV energy generation system.
- To integrate a standalone MPPT algorithm for the solar PV system this is linked to the DC link of the back-to-back ($\mathfrak{b}t\mathfrak{b}$) converters.
- To utilize the best wind MPPT algorithm to maximize the capture of wind energy in the region of the speed characteristics of wind turbines

This article is structured as described in the following section. In section 2 explains the renewable energy under investigation, including its hybrid system arrangement, modeling and its operation. Section 3 explains the controlling approaches of the hybrid wind-solar system to extract optimal power. Section 4 contains the simulation results for the proposed hybrid model and the conclusion is summarized in Section 5 of the article

Proposed wind solar hybrid model

In this research work, a solar integrated wind energy conversion system has been proposed (i.e. HWSES), where a DFIG is used to transform the wind energy into electrical energy which is integrated with solar PV system to the DC link of the back to back converters [17, 18] as shown in Fig. 1. Wind energy possesses energy in the form of kinetic energy. The extraction of this energy from the wind can be explained through the actuator disk theory based on energy balance equations and the application of Bernoulli's equation. There are certain assumptions taken into account while studying the theory of momentum and its behavior on wind turbines as shown in Fig. 2.

- The air is incompressible
- The fluid motion is steady

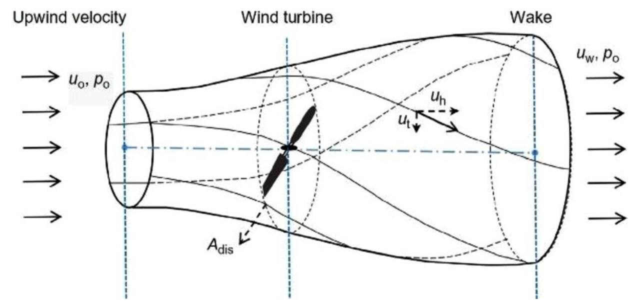

Fig. 2 Momentum theory/Actuator disk theory depicting the expansion of steam tube from the actual upwind/ axial wind velocity

- The variables have the same value for a given section of the air stream.

Solar radiation resources are determined by the earth's surface position, time and date of the day. These variables will contribute to evaluating the optimal amount of radiation. Other variables, including the elevation above sea level, the amount of water vapor or contaminants in the environment and cloud cover, all this contribute to decreasing the radiation amount below the optimum level. Although solar radiation may not undergo the same form of turbulence as wind, there may be short-term variations. Frequently, these

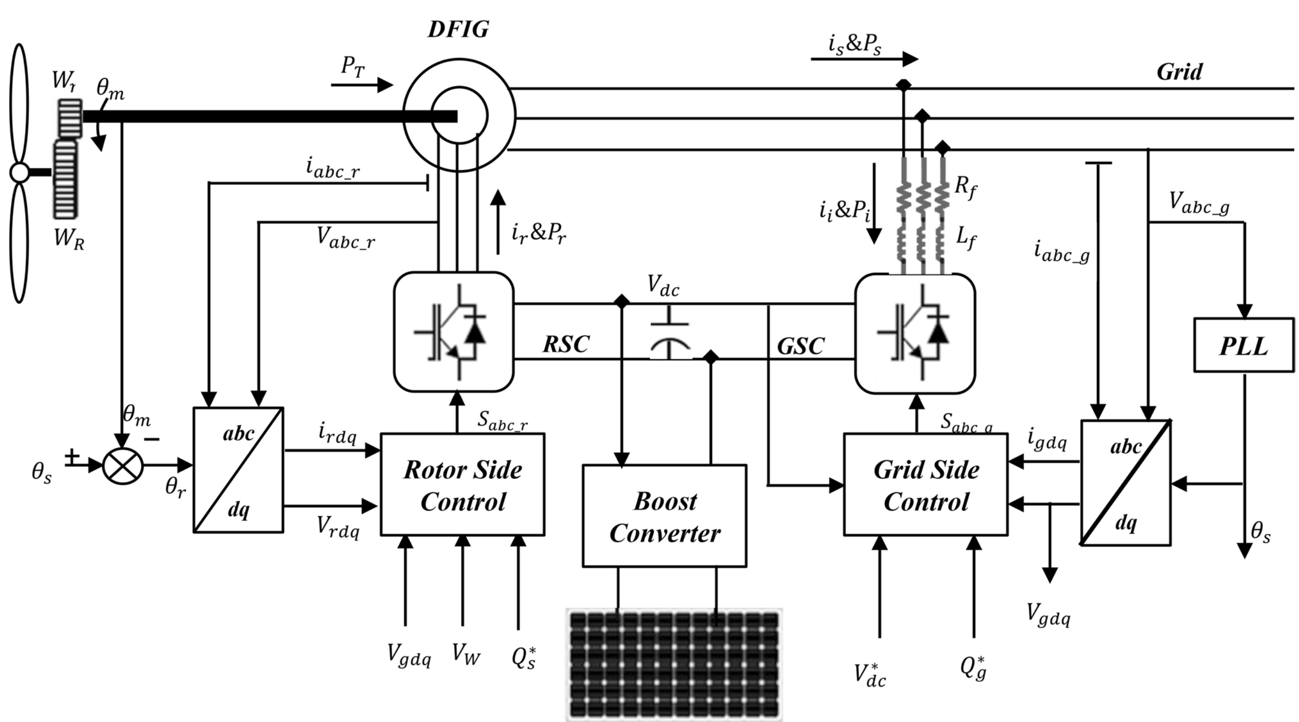

Fig. 1 ProposedHybrid wind-solar energysystem

are associated with the movement of clouds. Solar photovoltaic systems (PVS) have several benefits over wind energy systems (WES), including low maintenance requirements, the absence of moving parts and ease of installation

Modelling of wind turbine

Consider the wind turbine has a diameter D and it sweeps an area A, the available kinetic energy per unit time (wind power) when the wind speed is u *m/s* is [19]:

$$P_t = \frac{d}{dt}\left(\frac{1}{2}mu^2\right) = \frac{1}{2}u^2\frac{dm}{dt} \tag{1}$$

Considering wind speed to be constant for that particular interval of time. Thus, wind power depends upon the rate of change of air mass with respect to time. Equating air mass (m) with air density (ρ) and its volume (Q), it can deduce the wind power equation as:

$$P_t = \frac{1}{2}\rho Q u^2 \tag{2}$$

Replacing Q with Au, we get,

$$P_t = \frac{1}{2}\rho A u^3 \tag{3}$$

The wind turbine can recover only a part of this power. Hence, a dimensionless quantity is considered in the equation also called as coefficient of power $\left(C_p\right)$, which is a function of wind speed, rotational speed of the wind turbine and the pitch angle.

$$P_t = \frac{1}{2}\rho\pi R^2 u^3 C_p \tag{4}$$

C_p is a function of tip speed ratio (λ) shown by,

$$\lambda = \frac{R\Omega_t}{u} \tag{5}$$

Where R is the length of the turbine blades, Ω_t is the angular speed of the rotor [20].

There is a theoretical maximum limit where C_p can be considered (also called as Betz Limit), which is about 59.3% of the total power drawn from the wind. The rotor torque is obtained from the wind power and the speed of rotation of the turbine as shown in equation.

$$T_t = \frac{P_t}{\Omega_t} = \frac{\rho\pi R^2 u^3 C_p}{2\Omega_t} = \frac{\rho\pi R^3 u^2 C_p}{2\lambda} \tag{6}$$

$$T_t = \frac{\rho\pi R^3 u^2 C_t}{2} \tag{7}$$

Where C_t is coefficient of torque that is related to coefficient of power by the equation shown below and displayed in Fig. 3.

$$C_p(\lambda) = \lambda.C_t(\lambda) \tag{8}$$

DFIG is a wound-rotor / slip ring induction generator that has its rotor connected to a variable frequency source. By varying the rotor current frequency, we can capture the wind power at sub-synchronous and super-synchronous wind speeds. Thus, allowing the DFIG to generate power at variable speeds.

To obtain a variable frequency source, $\mathfrak{b}t\mathfrak{b}$ converters are connected between the grid and the rotor of the DFIG via DC link. The converters used are voltage source converter having bidirectional switches. Each converter has three legs, where each leg connects to each phase of the three-phase system. The key objective of the Grid Side Converter (GSC) (converter connected to the grid) is to regulate the reactive power consumed by the rotor of the DFIG to produce rotor flux and to keep a continuous DC bus voltage of the system [21] as shown in Fig. 4.

The main objectives of the Rotor Side Converter(RSC) (converter connected to the rotor) is to inject the three-phase voltage into the rotor at slip frequency, to maintain the stator power factor and to maximize the DFIG power by using the MPPT algorithm as shown in Fig. 5. Thus, these converters are responsible for bidirectional power flow in the system.

The control of these converters is very important for generating the rated voltage and frequency and to regulate the reactive power movement in the system. Hence, stator flux-oriented control is utilized to regulate the GSC and RSC. In this controller method, both stator and rotor

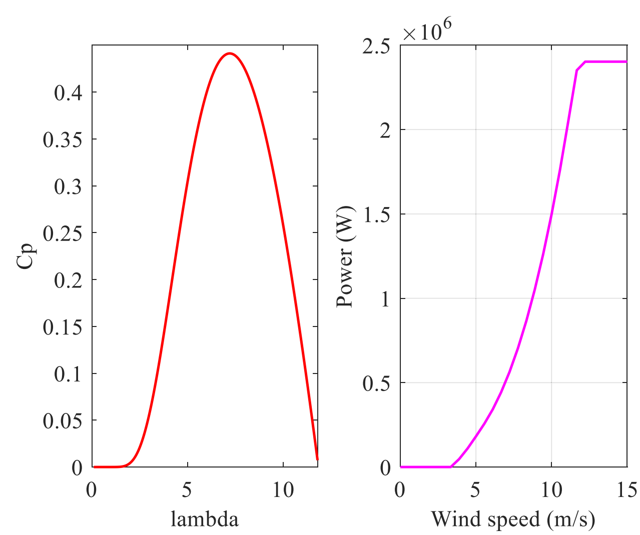

Fig. 3 Graphs of C_p Vs lambda and Power versus Wind speed

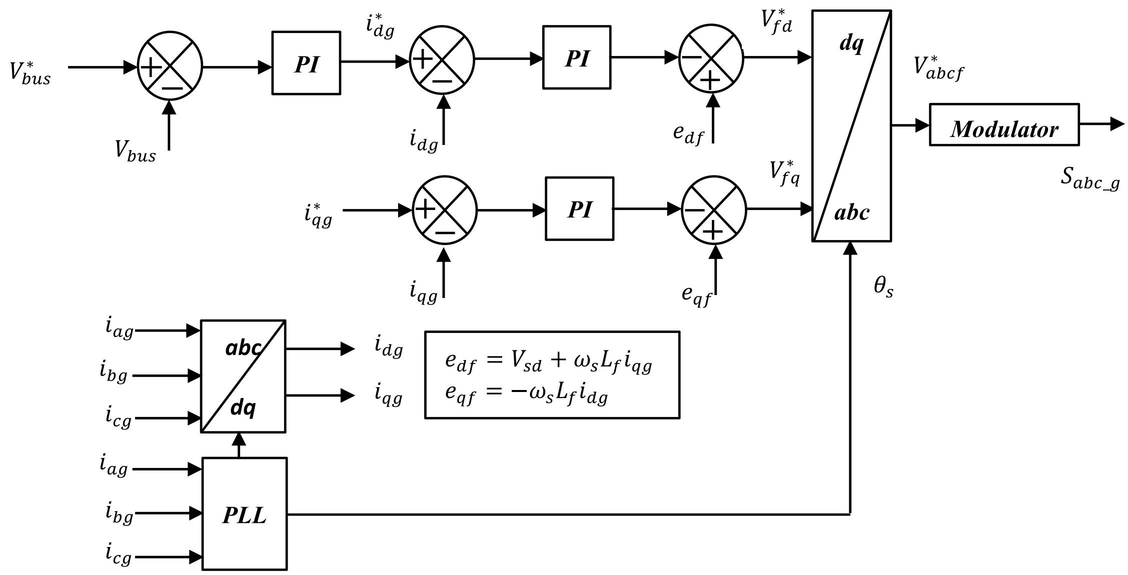

Fig. 4 Vector control analysis of Grid side controller

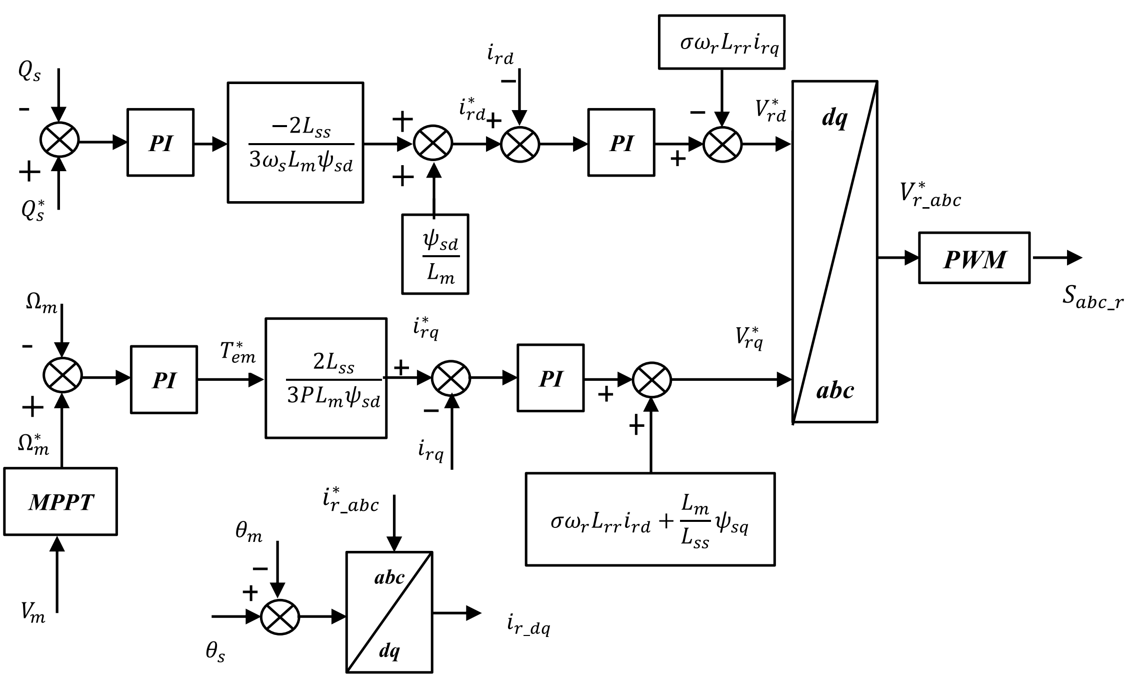

Fig. 5 Vector control analysis of Rotor side controller

rotating frames are converted into $d-q$ axes frames, which are rotating at synchronous frequency ω_s shown in Fig. 6.

By neglecting the saturation effect, the $d-q$ terminal voltage can be given as,

$$V_{sd} = R_s i_{sd} + \frac{d\Psi_{sd}}{dt} - \omega_s \Psi_{sq} \tag{9}$$

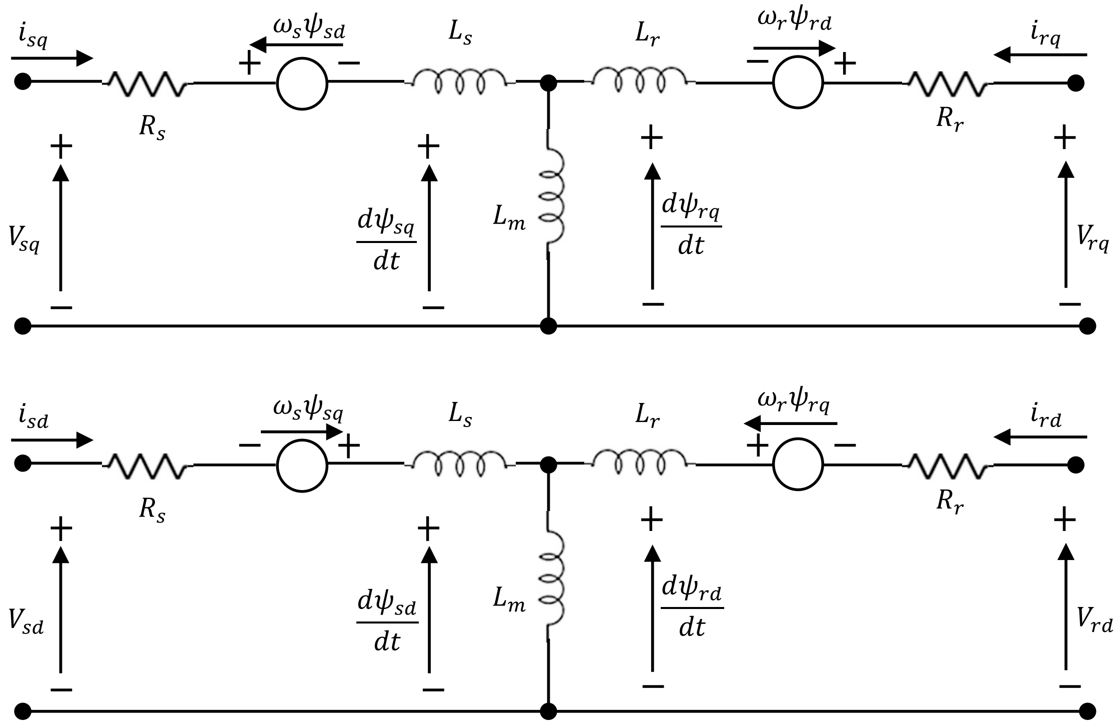

Fig. 6 Equivalent $d-q$ reference model rotating at synchronous speed ω_s

$$V_{sq} = R_s i_{sq} + \frac{d\Psi_{sq}}{dt} + \omega_s \Psi_{sd} \tag{10}$$

$$V_{rd} = R_r i_{rd} + \frac{d\Psi_{rd}}{dt} - \omega_r \Psi_{rq} \tag{11}$$

$$V_{rq} = R_r i_{rq} + \frac{d\Psi_{rq}}{dt} + \omega_r \Psi_{rd} \tag{12}$$

flux linkage equations,

$$\Psi_{sd} = L_{ss} i_{sd} + L_m i_{rd} \tag{13}$$

$$\Psi_{sq} = L_{ss} i_{sq} + L_m i_{rq} \tag{14}$$

$$\Psi_{rd} = L_m i_{sd} + L_{rr} i_{rd} \tag{15}$$

$$\Psi_{rq} = L_m i_{sq} + L_{rr} i_{rq} \tag{16}$$

Where, $L_{ss} = L_m + L_s$ & $L_{rr} = L_m + L_r$

Torque equation,

$$Te = 1.5p\frac{L_m}{L_s}(\Psi_{sq} i_{rd} - \Psi_{sd} i_{rq}) \tag{17}$$

The stator active and reactive powers are,

$$P_s = 1.5\left(V_{sd} i_{sd} + V_{sq} i_{sq} + V_{rd} i_{rd} + V_{rq} i_{rq}\right) \tag{18}$$

$$Q_s = 1.5(V_{sd} i_{sq} + V_{sq} i_{sd} - V_{rd} i_{rq} + V_{rq} i_{rd}) \tag{19}$$

Wind turbine speed control characteristics

Wind turbines are categorized according to the working speeds of the turbine i.e., fixed speed wind turbine (FSWT) and Variable Speed Wind Turbine (VSWT). FSWT operates at a limited angular velocity to deliver rated power, which accounts to 1.0% of the rated wind speed. If there is any variation in wind speeds, it will cause fluctuations in the output power.

VSWT operates a wide range of wind speeds with maximal transformation efficiency. In VSWT, the rotor speed is regulated to retain power at rated values although fluctuations in wind speed by the means of power converter systems.

The wind turbine speed-control characteristics are essential to keep the turbine speed in a safe operating mode and to reduce the mechanical stress on the drive train. Hence, wind turbine speed-control strategy is used based on 3 operating regions as shown in Fig. 7.

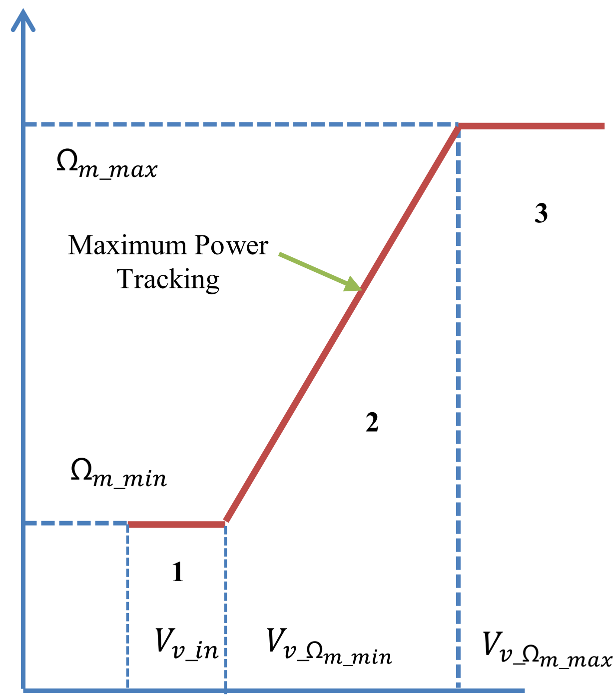

Fig. 7 Different operating regions of wind turbine based on its speed control strategy

- Minimum speed operating region
- Maximum Power Extraction region
- Maximum speed operating region at partial and full/rated power output region

Region 1 and Region 3

The key objective of these regions is to continue the turbine in its minimum value in region 1and maximum value in region 3. When the wind speed is relatively low, the turbine also revolves at a low frequency. This lower-frequency correlates to the resonance frequencies of the tower. Prolonged or continuous running of the turbine at lower speeds excites the resonant frequency of the tower and it weakens the structures and breaks due to vibrations. Hence, there is a limit set for the turbine below which should not be operated.

When the wind speeds are at dangerously high levels, the turbine speeds are to be limited to maximum safe operating levels as higher speeds cause inertial and centrifugal forces to act on the wind blades and turbine shafts, which breaks/damages the structure completely. Hence, the turbine is operated within the maximum safe operating limits.

Power maximization is not of importance in these regions and the only emphasis is to maintain the speeds in this region.

Region 2

In this region, the main objective is to extract optimum power. When the wind speed increases within this region the rotational turbine speed also increases linearly to attain maximum power extraction in this region. To attain the maximum power MPPT strategies are used with different types of controllers. One, by taking electromagnetic torque as a reference, which intern tracks the maximum power point. These types of controllers are called Indirect Speed Controllers (ISC). Second, by generating optimal turbine rotation speed (Tip speed ratio method) for each wind speed value and use this as the rotational speed reference. This type of controller is called direct speed controllers (DSC).

Solar PV modelling

Photovoltaic cells absorb photon energy (Light energy) and generate pollution-free electricity through the photoelectric effect. When photons are incident on the surface of the semiconducting material, it absorbs photon energy creating excess electron-hole pairs in the material. As each cell is doped to create an electric field at the junction (PN junction), the current flows only in a particular direction and blocks its flow in another direction. Thus, photovoltaic cells can be ideally represented by an ideal current source parallel to a diode.

This model is also called a single diode PV module equivalent circuit, which includes resistive elements (one in series and in parallel) accounting for power loss. A series resistance resembles the losses that occurred due to joule's effect, which is due to metal grids, connector bus and semiconductor material. A parallel resistance also called as shunt resistance is associated with current seepage in a cell due to cell thickness and surface effects. The effects of series resistance are predominantly due to the multiplication of cell resistance in the PV module

Output current expression of a PV cell

When a constant irradiance is illuminated on a PV cell, then J_{PV} is the current density generated in that particular volume of the cell. If the cell has an area A_{cell}, then the current generated by the PV cell is due to irradiance is,

$$I_{PV} = J_{PV} * A_{cell} \tag{20}$$

The output current I is,

$$I = I_{PV} - I_d - I_{sh} \tag{21}$$

Where, I_d is the diode current flowing through the parallel diode and I_{sh} is the shunt current flowing through the parallel resistor.

By, Shockley diode calculation the current that flows via the diode is [22],

$$I_d = I_0 * \left\{ \exp* \left[\frac{q * V_J}{nkT} \right] - 1 \right\} \tag{22}$$

Where,

I_0 is reverse saturation current (A)

n is diode ideality factor where 1 is for ideal diode

q is the elementary charge

k is Boltzmann's constant and T is the absolute temperature of the diode

At 25 °C, $\frac{kT}{q}$ is approximately equal to 0.0259 volts

From the figure, using Ohms law we can deduce that

$$V_J = V + IR_s \tag{23}$$

Where

V_J is the voltage through both diode and shunt resistor R_{sh}

V is the voltage over the output ports

R_s is the series resistance

and,

$$I_{sh} = \frac{V_J}{R_{sh}} \tag{24}$$

Substituting all the equations to the output current equation,

$$I = I_{PV} - I_0 \left\{ \exp \left[\frac{q(V + IR_s)}{nkT} \right] - 1 \right\} - \frac{V + IR_s}{R_{sh}} \tag{25}$$

Boost converter

The voltage produce by the solar PV panel is not a constant voltage as it is reliant on the solar irradiation and the temperature of the module. As these quantities vary for each instant of time, the output voltage also varies when these changes. In addition, the DC link bus of the back-to-back (𝔟𝑡𝔟) converter must always be constant hence; we cannot connect the PV module directly to the DC bus. A step-up DC-to-DC converter is setup to increase the DC voltage of the solar PV module and match with the DC link. A boost converter is one of the simplest switch modes step-up converters, which is connected in between the solar PV modules and the DC link off the 𝔟𝑡𝔟 converters.

A boost converter consists of an inductor, a switching device (MOSFET/IGBT), a diode and a capacitor. This converter steps up the DC voltage at its output without changing the input power.

The switches are the most important device required for the conversion of the voltages. Hence, the selection of the switches depends upon the operating voltage and switching frequency. IGBT is used as a switching device as we are more concerned about the output voltage and the performance characteristics of the switch. The duty cycle D of the IGBT switch determines the output voltage and its output voltage is expressed as,

$$V_{out} = \frac{V_{PV}}{(1 - D)} \tag{26}$$

The MPPT algorithm determines the duty cycle D, which is given as a gating pulse to the IGBT.

Optimization techniques for HWSES

The following section describes and analyzes the two MPPT techniques for the Hybrid Wind-Solar Energy System (HWSES).

Wind MPPT

The main objective of the wind turbine operating in region 2 of the turbine speed characteristics is to capture the maximal wind energy from the wind using MPPT. It could be obtained by taking the actual wind speed as a reference to the controller (DSC) or by taking the torque as reference (ISC) [23].

Tip speed ratio

The wind turbine's TSR is determined by the mechanical arrangement of the turbine and to maximize the C_p value through changing the blade structure. The maker of each wind turbine will provide the correlation betwixt the TSR, the C_p and the blade pitch angle.

This correlation is contributed for the wind turbine utilized in this article.

$$C_p(\lambda, \beta) = c_1 \times \left(\left(\frac{1}{\lambda + 0.080 \times \beta} + \frac{0.0350}{\beta^3 + 1} \right) \times c_2 - c_3 \times \beta - c_4 \right) \times e^{-\left(\frac{1}{\lambda + 0.080 \times \beta} + \frac{0.0350}{\beta^3 + 1} \right) \times c_5} + c_6 \times \lambda \tag{27}$$

Where β indicates the angle of the blade pitch (β = 0 is specified to the MPPT controlling region), c_1, c_2, c_3, c_4, c_5 and c_6 are the constant coefficient that depend on the blade's mechanical arrangement and λ denotes the TSR.

Choosing the coefficient values are $c_1 = 0.30$, $c_2 = 100$, $c_3 = 0.40$, $c_4 = 7.0$, $c_5 = 13.0$ and $c_6 = 0.01050$, then TSR is presented in Eqs. 5. Examining Eqs. (4)– (5) and Fig. 3, it is explicit that the WT has a distinctive optimum TSR value for

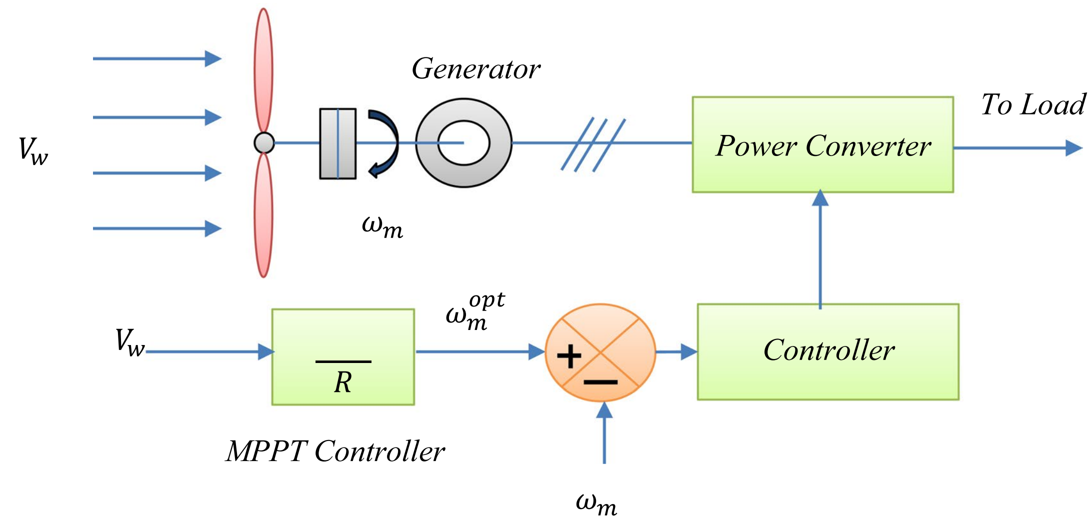

Fig. 8 Tip speed ratio MPPT technique implemented to the region 2 of the wind speed curve characteristics.

maximizing power. Thus, in this method, the optimal angular rotation of the machine is taken as a product of optimal TSR and the wind speed as shown in Fig. 8.

Optimal Torque method (OT)

The optimal torque control algorithm is a control algorithm that uses the proportional integral controller, which controls the torque of the wind turbine, which is relative to the square of the angular rotation of the wind turbine.

Unlike TSR, this method does not use an anemometer to record the wind speed, as these measurements are inappropriate, tedious and are not accurate wind speed measurements. The key objective of this method is to obtain the maximal operating point without using wind speed measurements.

At maximum power point,

$$\lambda_{opt} = \frac{R\Omega_t}{u} \tag{28}$$

$$C_p = C_{pmax}, C_t = C_{topt} \tag{29}$$

By equating the optimal TSR value to the torque extracted by the turbine equation, we get

$$T_t = \frac{\rho\pi R^3 C_t}{2} * \left(\frac{R\Omega_t}{\lambda_{opt}}\right)^2 \tag{30}$$

$$T_t = \frac{\rho\pi R^3 C_{p\max}}{2\lambda_{opt}}\left(\frac{R^2\Omega_t^2}{\lambda_{opt}}\right) \tag{31}$$

$$T_t = \frac{1}{2}\rho\pi\frac{R^5}{\lambda_{opt}^3}C_{p\max}\Omega_t^2 \tag{32}$$

$$T_t = K_{opt}\Omega_t{}^2 \tag{33}$$

Where,

$$K_{opt} = \frac{1}{2}\rho\pi\frac{R^5}{\lambda_{opt}^3}C_{p\max}\Omega_t^2 \tag{34}$$

In this technique, an optimal torque value T_{opt} is taken as a reference torque and is compared with the present torque value. The difference between these torques values are taken as an error signal to the PI controller. This controller feedbacks the updated torque value to minimize the error signals as shown in Fig. 9.

This approach is the fastest and most efficient method of tracking the maximum operating power point of the wind turbine, as no wind measurements are required.

Solar MPPT

A solar PV cell has nonlinear $I - V$ characteristics and the output power relies on the climate circumstances such as solar irradiation and temperature. Thus to extract optimum power from the sun, MMPT algorithms are adopted to optimize the output power. Perturb and observe method is one such method that continuously tracks the output voltage and power of the solar PV method [24].

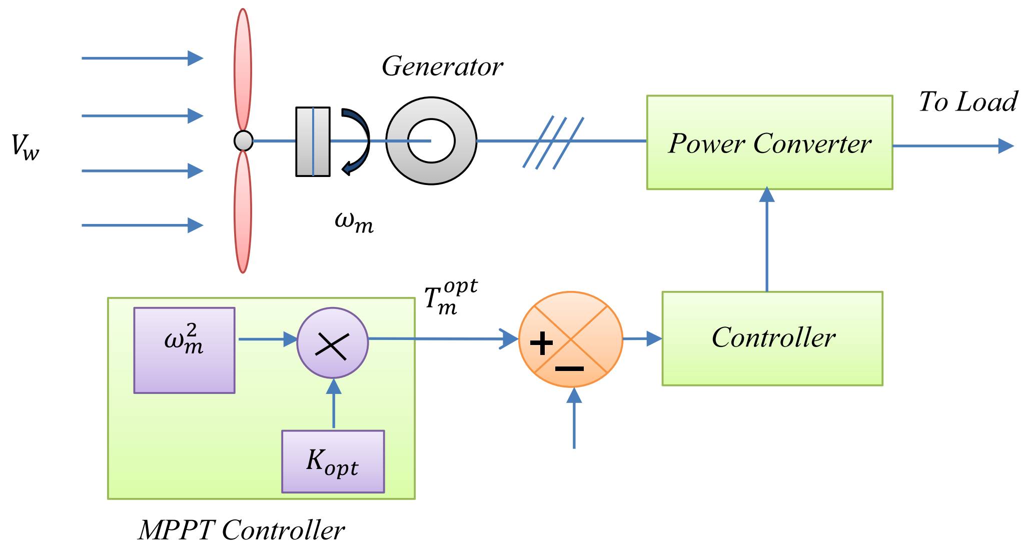

Fig. 9 Optimal Torque MPPT technique implemented to the region 2 of the wind curve.

Fig. 10 Power v/s Voltage curves of a solar cell.

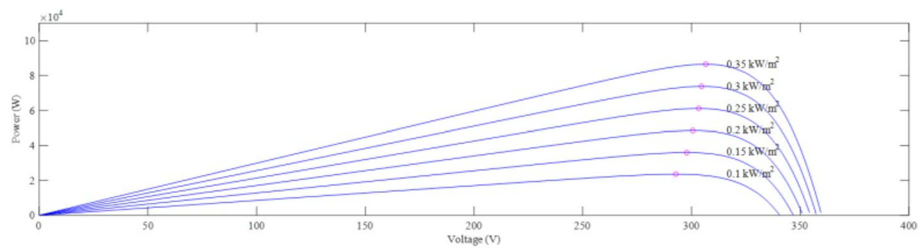

Perturb & observe algorithm

The Perturb & Observe (P&O) method is an arithmetic modelling method employed to seeking the optimal point of a specified function. This technique emphasizes to use a control parameter perturbing in slight increment size and finding the results in the aim function before the slope is zero.

The P&O technique periodically works by perturbing the voltage value and observing the power variations. This method continuously tracks the output power and voltage of the solar PV system.

As displayed in Fig. 10, if the operational point is to the left-hand side of the maximum point in the curve, the controller operates to the right, to get the maximum point. If the operational point is to the right-hand side of the maximum point, the controller operates to the left, to maximize the output. This mechanism can be obtained by taking the slope of the control variable with respect to the target variable [25].

In this algorithm, the voltage and the power is taken as the input from the PV array. When the operating voltage is perturbed and if the power increases, then the position has shifted toward the maximum power point. This process is continued till the power decreases. If the perturbed power decreases, then the operating position has shifted away from the MPP. Then the operating voltage should be perturbed in the opposite path. The movement of the operating point can also be determined with the help of slope of the power variation with respect to the voltage variation. In this way, the algorithm ensures the system to reaches maximum power operating point as shown in Fig. 11.

However, there is a trade of to be considered while taking the step size of the duty cycle, as large step size signifies that quicker response and additional oscillations throughout the peak point, which indicates lesser efficiency. If the step size is significantly smaller, the efficiency increases but greatly decreases the convergence speed.

Incremental conductance algorithm

Incremental conductance (IC) algorithm is a mathematical optimization algorithm used to track the optimal point on a $P - V$ curve by taking the slope of the power and the voltage of the PV array and equating it to zero. When this condition satisfies, then the point obtained is the MPP.

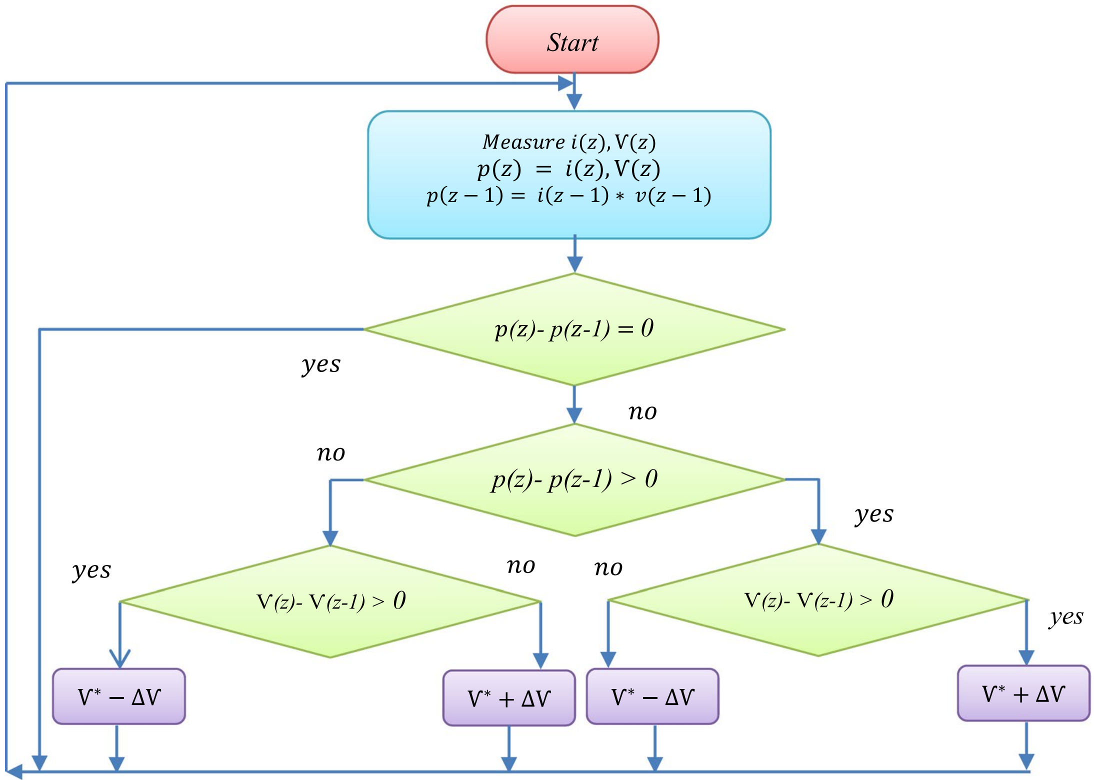

Fig. 11 P&O algorithm to extract Maximum power point.

When the slope of the PV array is greater than zero then the point is toward the left of the MPP [19]. When the slope of the PV Fig. 12 array is lesser than zero, then the point is toward the right of the MPP. With proper gating pulse to the system, we can obtain the optimal point.

From Fig. 13, at MPP,

$$\frac{dv}{dv} = \frac{d(v * I)}{dv} = 0 \tag{35}$$

On differentiating power with respect to voltage [26], we have

$$I + v\frac{dI}{dv} = 0 \tag{36}$$

Dividing the equation by V and equating the above equation, we get

$$\frac{dI}{dv} = -\left(\frac{I}{v}\right) \tag{37}$$

The ratio of change in incremental current with respect to incremental voltage in a PV array is equal to the negative of the conductance of the solar PV array at MPP. Thus, the conductance of the system can determine the maximum operating point of the system.

When the operating point is located in the left side of the MPP, then the equation $\left(\frac{I}{V} + \frac{dI}{dV}\right)$ is greater than zero. When the operating point is on the right side of the MPP, the equation $\left(\frac{I}{V} + \frac{dI}{dV}\right)$ is less than zero. Thus, the system can detect the position and perturb toward the MPP with the help of voltage as shown in flowchart in Fig. 12

Solar PV Simulink model

The solar PV power system is attached to the DC link of the btb converter as the DC power generated can be directly fed to the grid without connecting any extra inverter.

A standalone solar PV system is simulated in a Simulink model using different MPPT strategies. To choose the best MPPT algorithm for a standalone solar PV system, a Simulink model of this system is created which is linked to the boost converter as shown in Fig. 14. The variation of power, voltage and current of solar PV system as shown in Fig. 15.

DFIG wind turbine simulink model

The Wind turbine model consists of computational equations that convert the wind speed to its equivalent torque and feeds to the DFIG machine. As the wind turbine rotates,

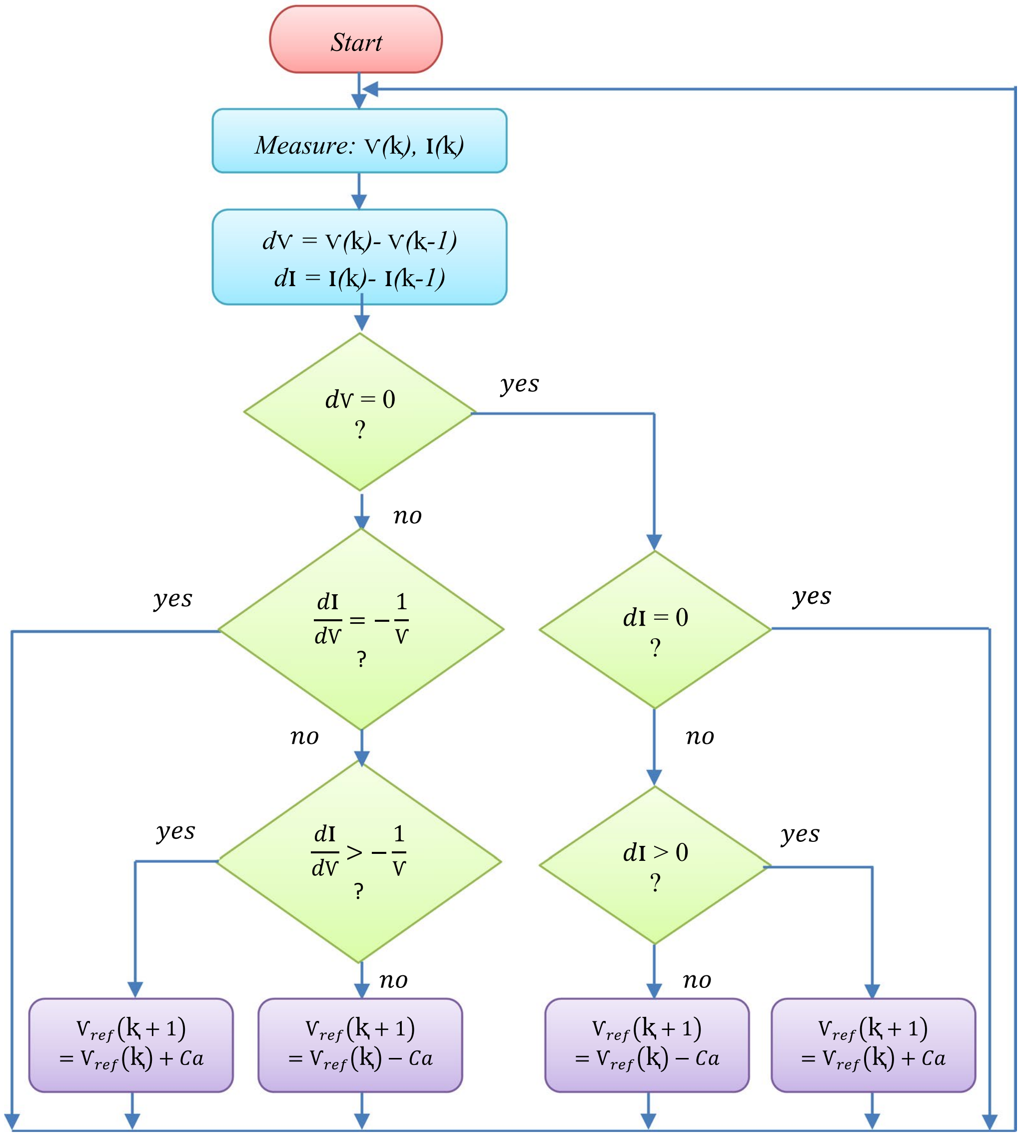

Fig. 12 Flowchart of IC MPPT system

these fluxes dynamically induce the EMF in the stator of the DFIG and generate electricity.

This controller consists of the MPPT controller that inputs the wind speed and feds to the PI controller. The output of the PI controller is converted into the $d - q$ axis and fed as the switching pulses to the rotor side controller as displayed in Fig. 16.

The reactive power is by the rotor winding of the DFIG machine, which is controlled by the grid side converter to generate rotor flux. This process is observed during the starting of the DFIG.

The above Fig. 17 is a grid-side controller circuit, which takes the V_{bus} as the input and is fed to the PI controller. That signal is converted into switching pulses using the stator vector control method.

These controllers are fed to their respective converters to generate power. The power generated can be maximized by using different MPPT algorithms. We have modelled Tip speed ratio (TSR) model and the Optimal Torque MPPT algorithm to the hybrid wind-solar conversion system. Here all the variable parameters of the model are kept constant and only the MPPT's are varied keeping the wind speed constant. Thus the power generated by each algorithm determines the best MPPT algorithm for the hybrid wind-solar conversion system.

Under running conditions, the rotor generates electricity, which accounts to 30% of the total power generated.

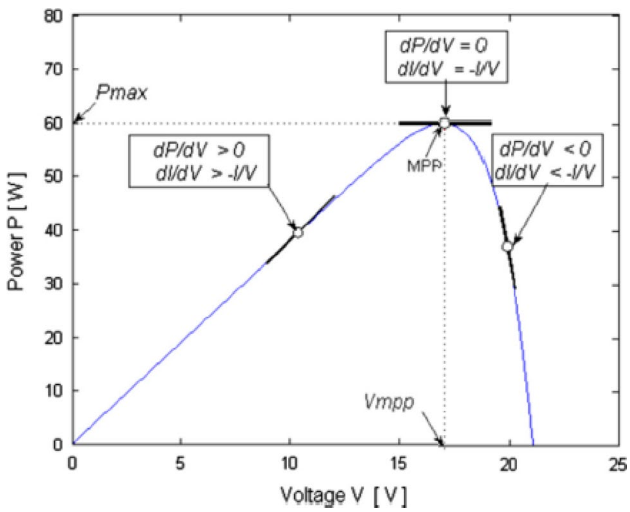

Fig. 13 Power versus Voltage graph of a solar cell indicating different MPP points

Results and discussion

The proposed model consists of a wind solar hybrid model is simulated using MATLAB Simulink environment as shown in Fig. 18

The proposed model consists of a wind turbine model, DFIG machine, 𝔟𝔱𝔟 converter, a grid filter and a transformer. The stator connections of the DFIG id linked to the grid, while rotor connections of the DFIG machine is linked to the grid using a transformer and 𝔟𝔱𝔟 converter as shown in Fig. 18.

Solar PV MPPT validation for HWSES

Trina Solar TSM-0250PA05.38 is the module used for simulation. The Detailed Solar device parameters are specified in Table 1.

P&O and IC MPPT techniques have been implemented to this system and comparison of their efficiencies have been noted.

By keeping all the parameters of the standalone solar energy system to its previous values and only changing the MPPT algorithms, we obtain graphs is displayed in Figs. 19 and 20. From the efficiency graphs shown in Figs. 19 and 20, we can see large spikes at 0.5 sec and from 3.5 to 4 sec. This indicates that the system is instable while searching for a maximum power point. This also indicates the system to be highly sensitive to any type of noises, creating local maxima points, there by delaying the expected output. Thus from the graphs, we can clearly

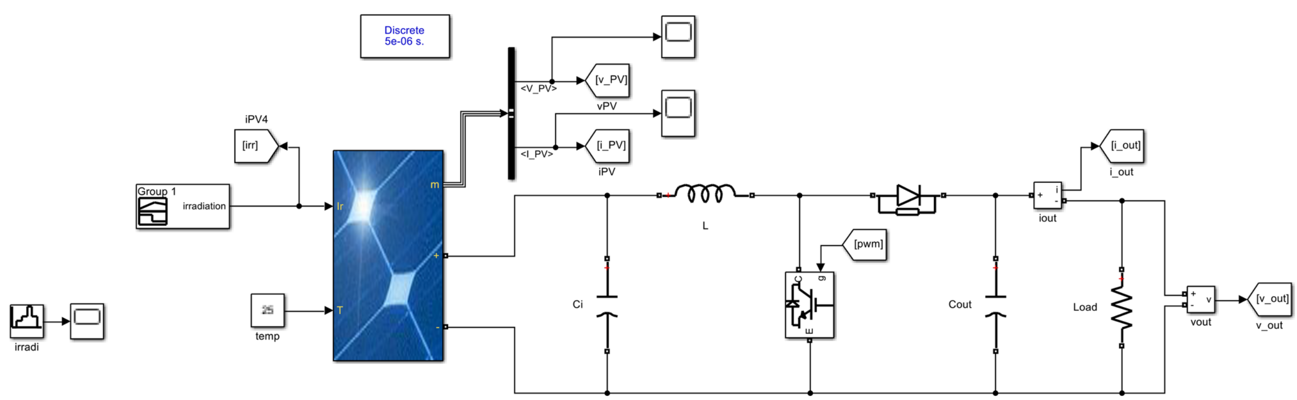

Fig. 14 Solar energy conversion system connected to the grid.

Fig. 15 Graphs indicating the variation of current and power v/s voltage in a solar cell.

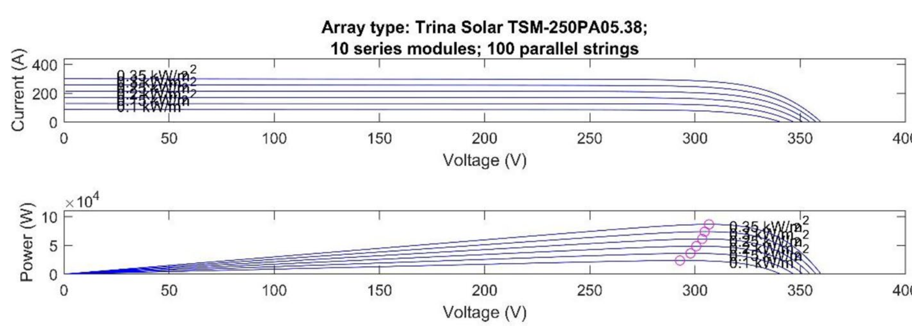

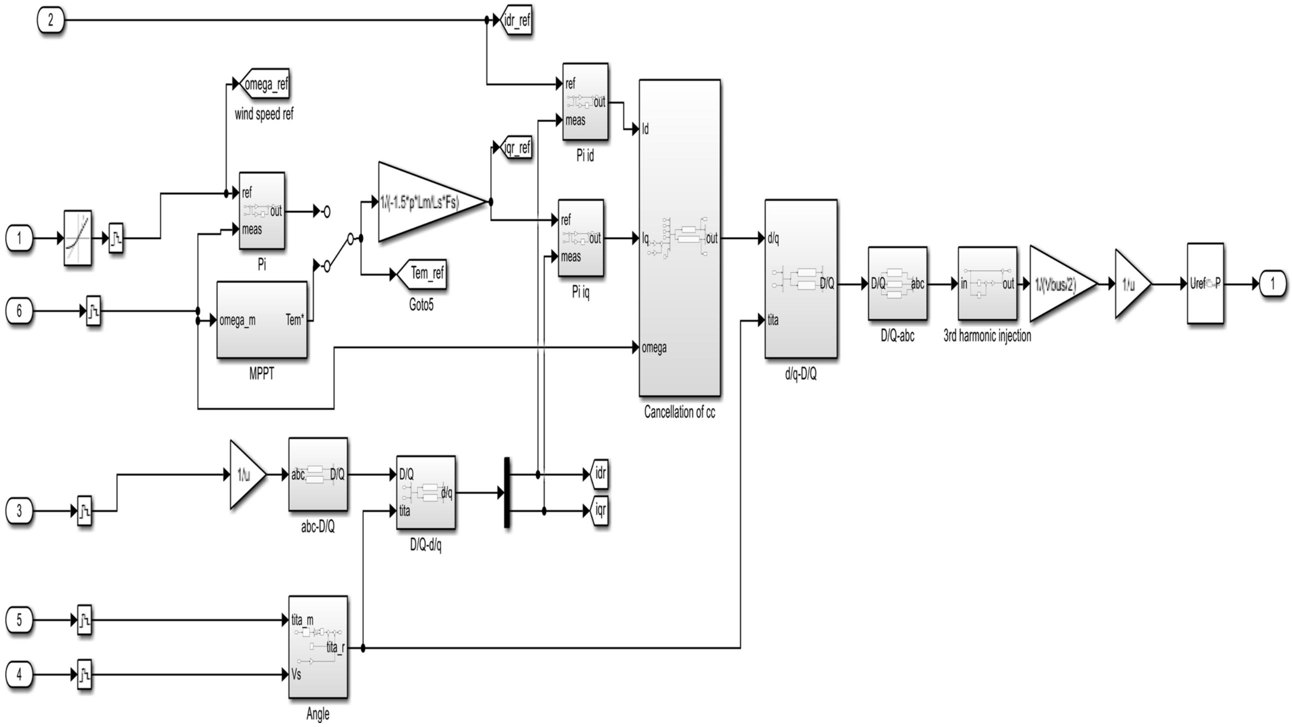

Fig. 16 Vector control simulink model of rotor side converter

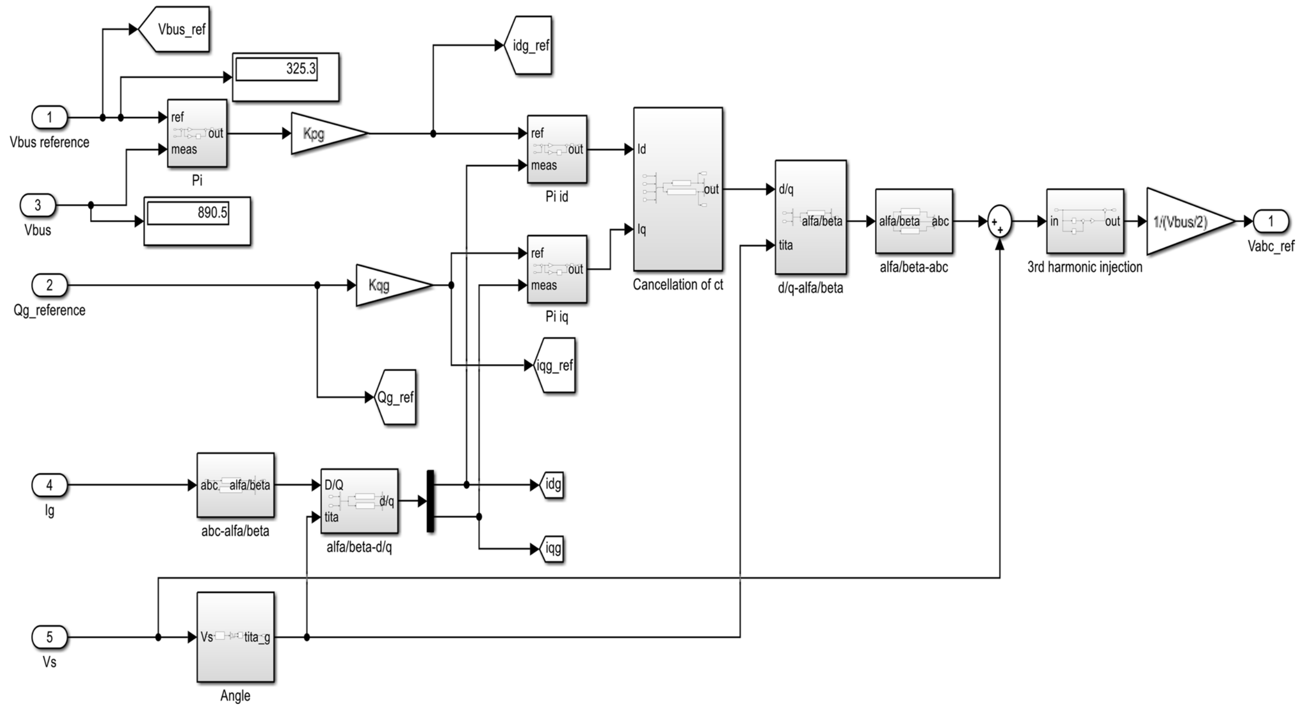

Fig. 17 Vector control simulink model for grid side converter

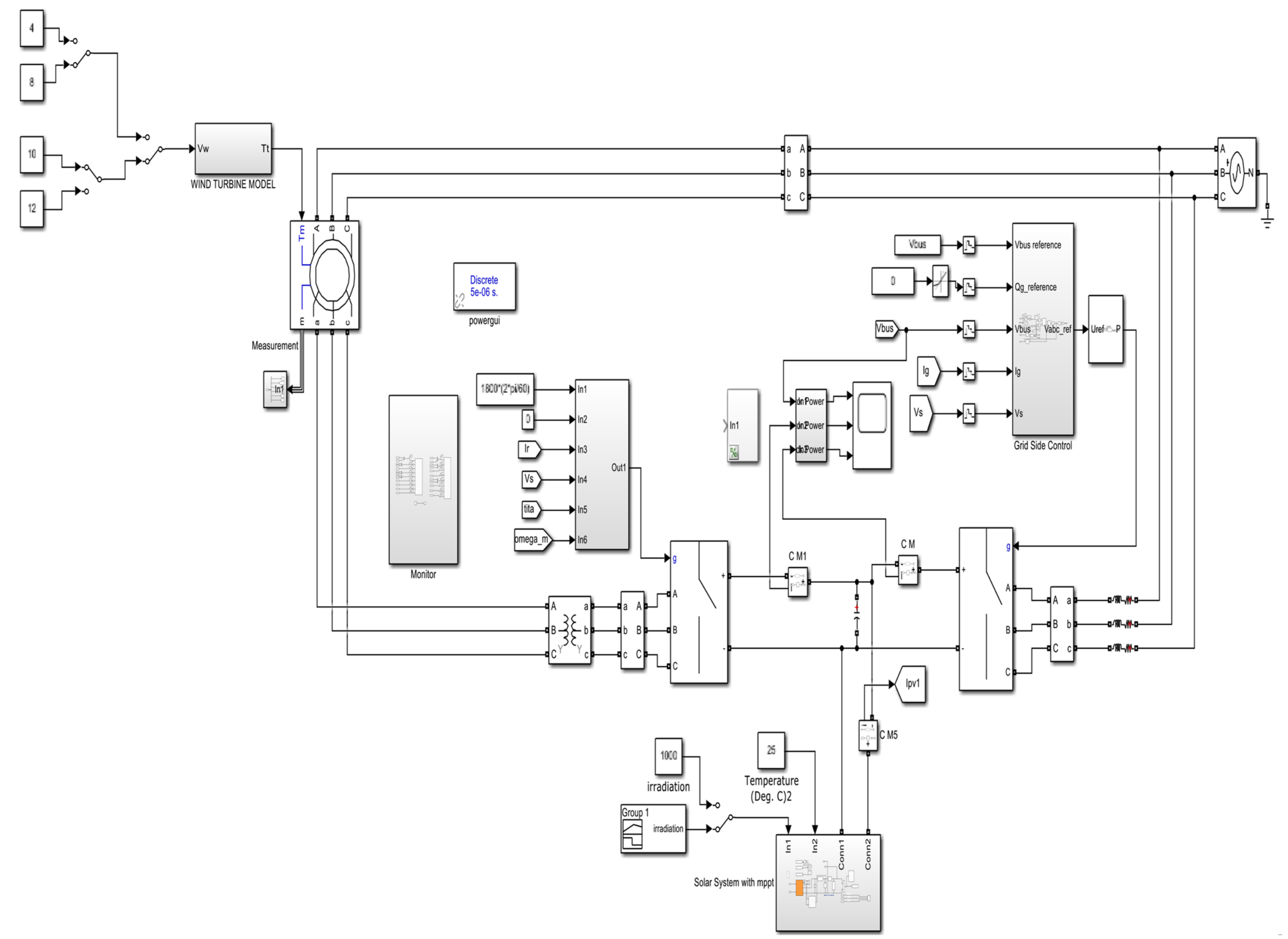

Fig. 18 Simulated model of hybrid wind solar conversion system.

Table 1 Solar array parameters

Parameter	Value
Maximum Power (P_{max})	0.24986KW
Maximum Current (I_{max})	31.5V
Maximum Voltage (V_{max})	8.16A
Open Circuit Voltage (V_{OC})	8.56A
Short Circuit Current (I_{sc})	0.03760KV
Series connected modules per string	36
Parallel strings	20

The graphs also indicate that the perturb and observe method has better efficiency as it is observed that the mean efficiency of the P&O methods is 94.5% whereas the incremental conductance mean efficiency graphs shows 94.35%. Thus, a substantial increase of 0.15% in its efficiency and the advantage of stability toward noises and the ability to clear the faults at a shorter period confirms that the P&O method is better.

Considering the above result, the solar PV system is integrated into the proposed hybrid system with Perturb and Observe MPPT algorithm using MATLAB Simulink model.

DFIG wind turbine MPPT validation for HWSES

The proposed model is run for different wind speeds and the complete variation of the parameters such as torque, wind speeds, currents and voltages are indicated in the graphs.

The Detailed DFIG device parameters are specified in Table 2.

Sub synchronous speed

The hybrid system is modelled to run at a wind speed of $4m/s$ which simulates the system to run at sub synchronous

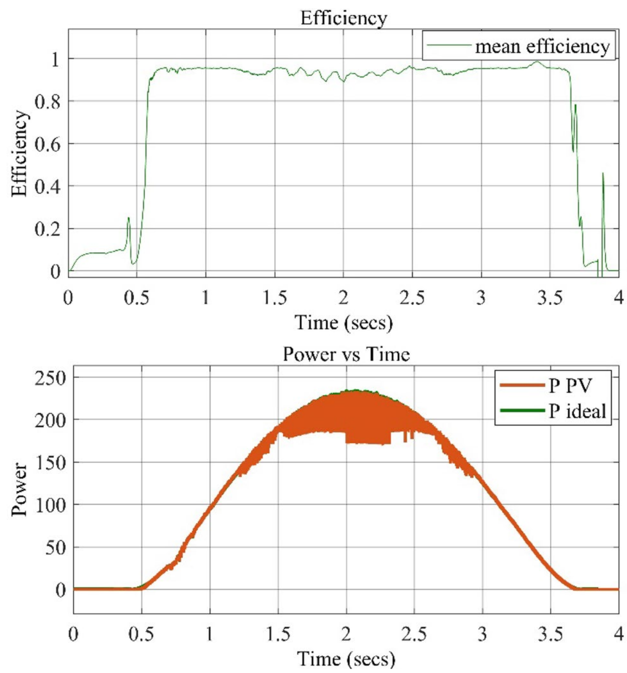

Fig. 19 Plots indicating the efficiency of the solar cell and ideal and actual power generated from the solar cell using perturb and observe MPPT algorithm.

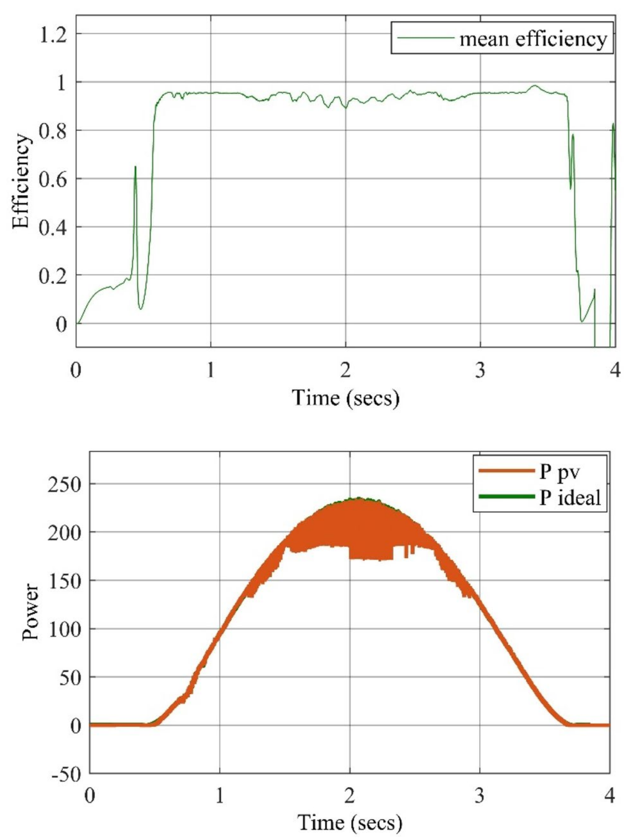

Fig. 20 Plots indicating the efficiency of the solar cell and ideal and actual power generated from the solar cell using Incremental Conductance MPPT algorithm

Table 2 DFIG Parameters

Parameters	Value
Rated Power (P_{rated})	2.0MW
Stator Current (I_s)	1.960KA
Stator Voltage (V_{stator})	0.690KV
Rated Torque (T_{rated})	12732Nm
Rated Rotor Voltage	2.070KV
No of Pole pairs	2
Working frequency	50Hz
Switching frequency	4KHz
DC bus voltage	1.150KV
Speed of the Rotor shaft	1500RPM
L_m	2.5mH
σ	0.087mH
R_s	2.6mΩ
R_r	2.9mΩ

speeds. The power graphs are shown in Figs. 21 and 22, depicting different MPPT algorithms.

From Figs. 21 and 22, we can see a noticeable difference in the figure after 3 seconds. Figure 21, obtained from running the system in sub synchronous speed using OT algorithms, has stabilized after 3 seconds and tries to feed a constant power to the grid. Whereas, in Fig. 22, just after the 3 sec, there is a considerable bulge in the power, for a very short period of about 1 sec. This indicates the system takes a longer duration to stabilize the system when there are fluctuations in the system.

Figs. 23 and 24 indicate the rotor side parameters variation running at sub synchronous speed for OT and TSR algorithms, respectively. In the system, a unit ramp function is used to the speed input to depict the wind variations for a short interval of time. This causes a surge current in the rotor at 3rd and 4th sec in Fig. 24. However, when the same model is run using the OT method, no surges in rotor current takes place thus has a better response to the wind variations with respect to the frequency rather than the surge in the amplitude of the current. When the wind speed varies, the rotor current varies also varies to keep the stator voltage and current constant

Figures 25 and 26 shown above is a graph of grid side parameters and the variation of its values while running the OT and TSR algorithms for Maximum power extraction. The grid side converter is very essential to maintain the amplitude and frequency generated from the system to feed the grid. To do so, the bus voltage must be constant. If we look at the graph, the bus voltage has reached a constant value at 3.56 sec while using the OT MPPT algorithm, but when we

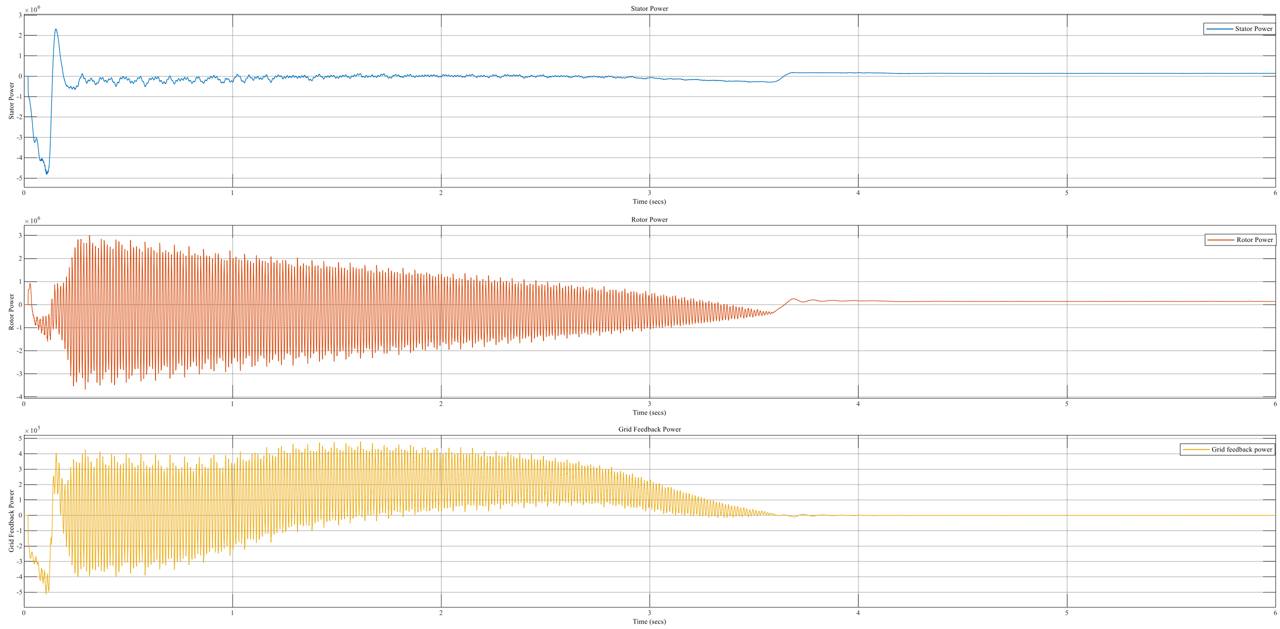

Fig. 21 Stator, rotor and grid feedback graphs of the system using Optimal Torque MPPT algorithm running at sub synchronous speed

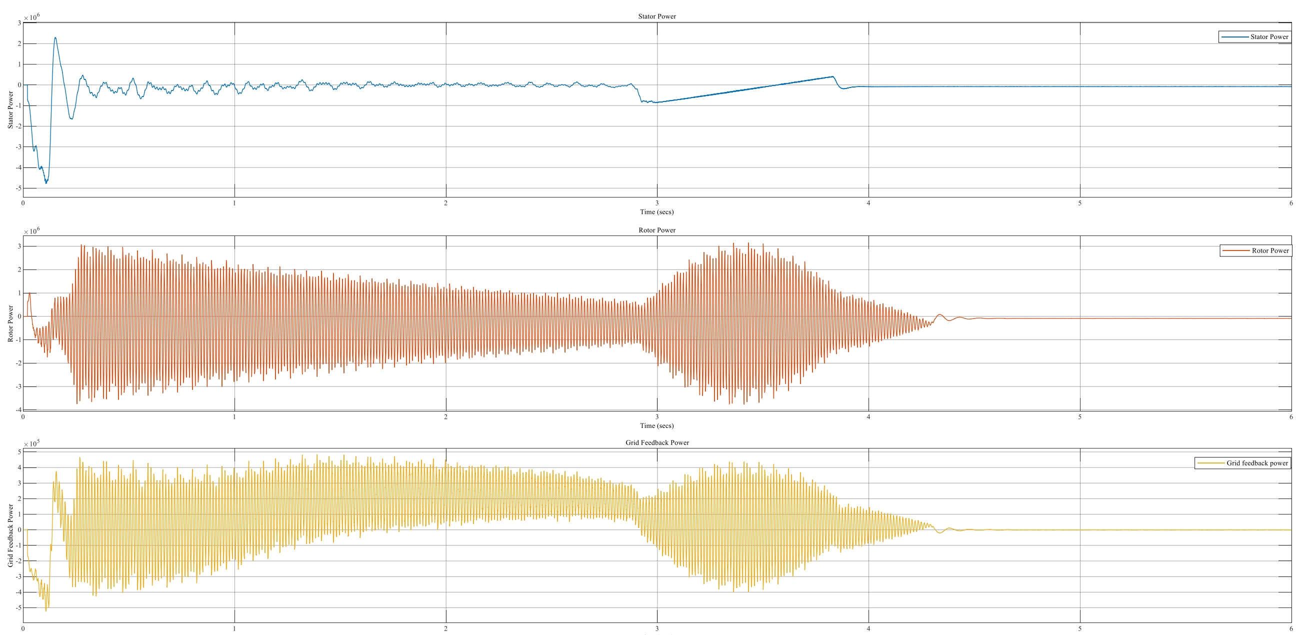

Fig. 22 Stator, rotor and grid feedback graphs of the system using TSR MPPT algorithm running at sun synchronous speed.

used the TSR algorithm, the bus voltage reaches the constant value only after 4.3 seconds. Thus OT method has a clear advantage in giving faster results and to optimize the system in shorter periods.

Synchronous speed

The hybrid system is modelled for the wind speed of $8m/s$, which is an ideal condition for wind power generation. The optimal torque MPPT algorithm is used and the output Stator

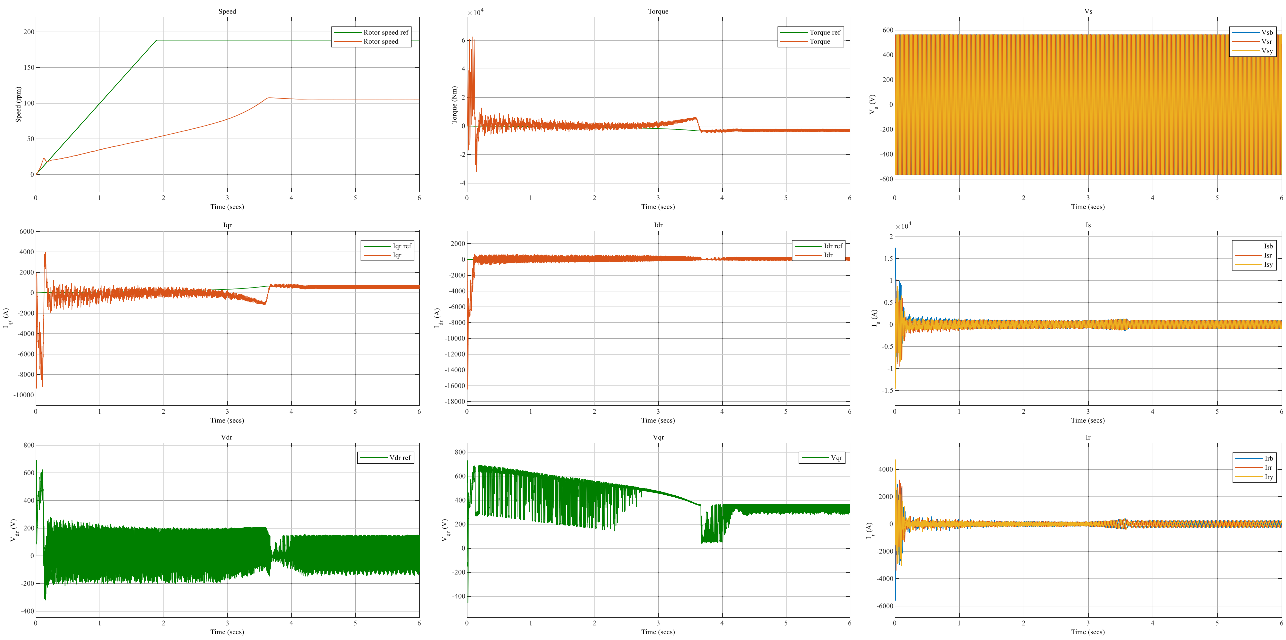

Fig. 23 Variations of Rotor side parameters like speed, torque, d-q axis voltages and currents, stator voltage and stator and rotor currents using OT MPPT algorithm running at sub synchronous speeds.

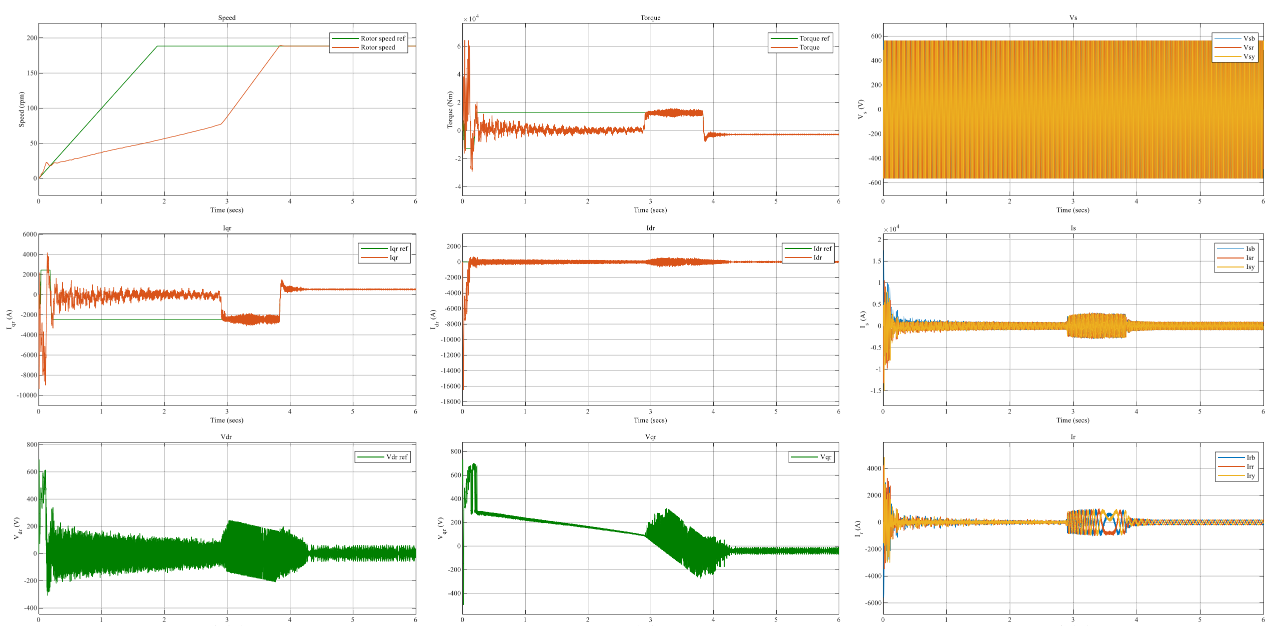

Fig. 24 Variations of RSC Parameters such as speed, torque, d-q axis voltages and currents, stator voltage and stator and rotor currents using TSR MPPT algorithm running at sub synchronous speeds.

power, rotor power and grid feedback power are shown in Fig. 27. In addition, the same model is modelled using TSR method as shown in Fig. 28.

At a time of 1.5 sec, the optimal torque MPPT algorithm stabilizes the system to generate constant power output through stator and rotor windings. Hence, we can see that after 1.5 sec, the stator power and rotor power generated is almost constant. From Figs. 27 and 28, it is evident that the hybrid system is showing a controlled response when the optimal torque MPPT algorithm is

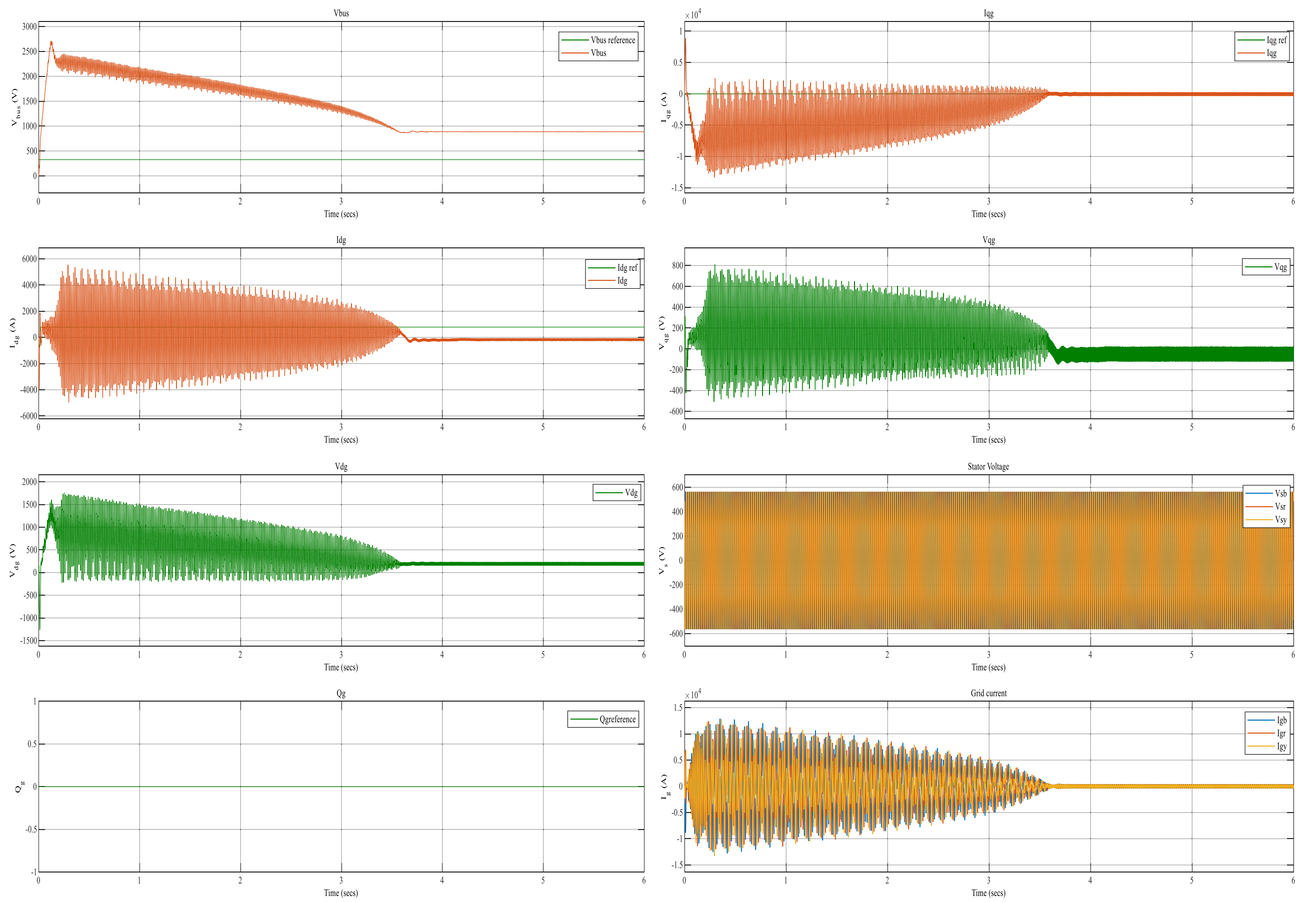

Fig. 25 Grid side parameter variations such as bus voltage, d-q axes voltage and currents, stator voltage and grid currents while using Optimal torque MPPT algorithm running at sub synchronous speeds

implemented. Under the TSR algorithm, the system has an uncontrolled response and there are huge variations in the output graph.

The above Figs. 29 and 30 has all the waveforms related to the rotor side converter, including speed, torque, direct and quadrature axis rotor side voltage and currents, Stator voltage and current and rotor currents.

Here in Fig. 30, there is a considerable amount of drop-in rotor current and stator current during the synchronous mode of operation of the DFIG machine. Whereas in Fig. 29, even in any type of mode there is no considerable drop in stator or rotor currents

In Fig. 32, the DC bus voltage after the initial voltage buildup starts increasing with respect to the TSR algorithm. This causes stress over the grid side converter as it has to feed constant AC sources to the grid with a particular frequency. This is achieved in the OT method as the bus voltage in this method remains in constant value so the grid voltage produces constant stator voltage to feed the grid as illustrated in Fig. 31.

Super Synchronous speed

The hybrid system is made to run at super synchronous speed and the variation of the stator, rotor and grid feedback power can be noted along with rotor side parameters and grid side parameters.

Figures 33 and 34 show the graph of stator power, rotor power and grid feedback power of the hybrid system running at super synchronous speed using OT and TSR algorithm.

Here the rotor and grid feedback power has huge variations as the turbine is rotating at super synchronous speed. The system running with the TSR algorithm has increased rotor and grid feedback power to keep the stator power constant and can be seen after 1.5 sec. But when it comes to the OT algorithm, the MPPT tries to make the stator power constant, along with rotor and grid feedback power.

Figures 35 and 36 show the rotor side converter control parameters and its variation with respect to time using OT and TSR MPPT algorithms. In Fig. 35, we have speed variation in the graph and accordingly, the rotor current

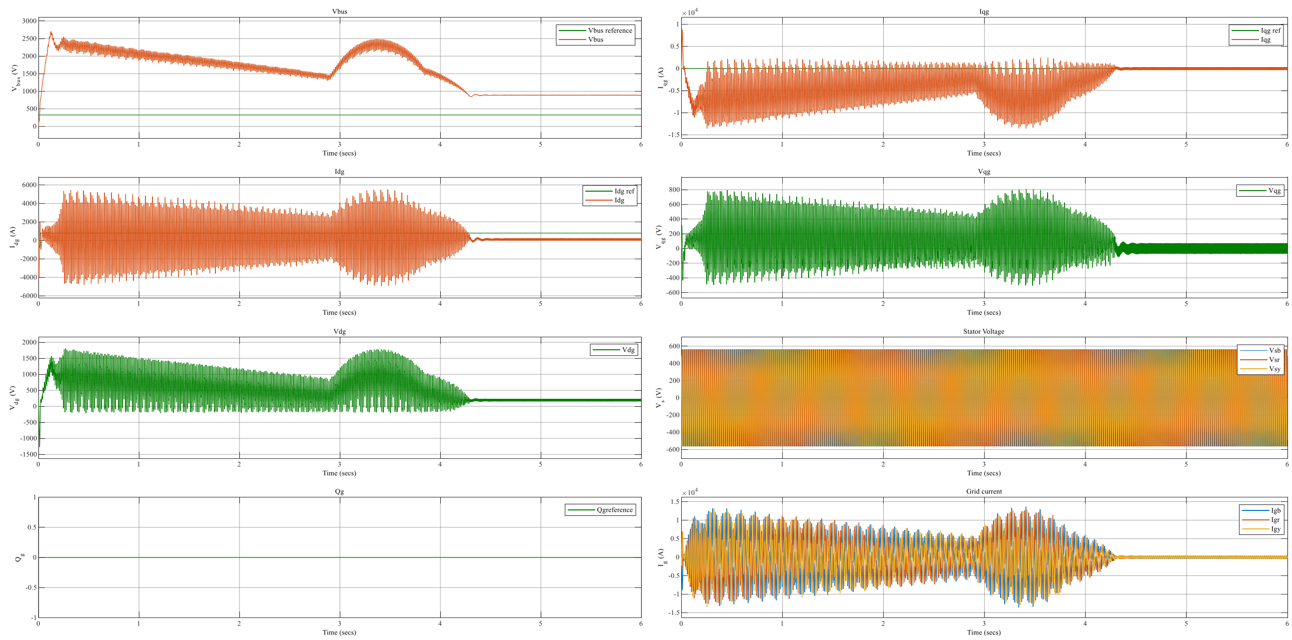

Fig. 26 Grid side parameter variations such as bus voltage, d-q axes voltage and currents, stator voltage and grid currents while using TSR MPPT algorithm running at sub synchronous speeds

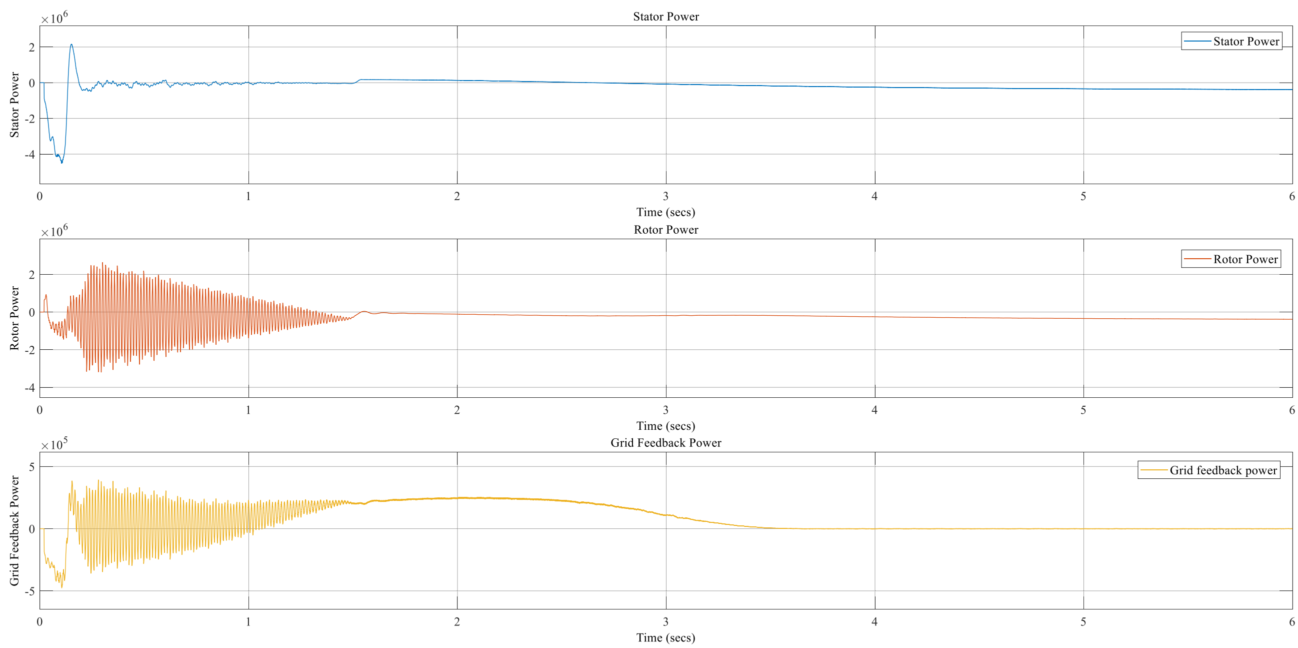

Fig. 27 Stator power, Rotor power and grid feedback power of the hybrid system for 8m/s wind speed using optimal torque MPPT algorithm running at synchronous speeds.

also changes to keep the torque and reactive power constant. Also, we can see a drop in the torque at time 2 sec in 36 which is the main reason the rotor current doesn't change even if the speed changes. The $d-q$ axes voltage and current changes according to the torque of the rotating system and as there is a drop in torque at 2 sec, we can see variations in $d-q$ voltages and current.

Figures 37 and 38 show the grid-side control parameters of the hybrid system, running at super synchronous speed using OT and TSR MPPT algorithm. In the TSR method,

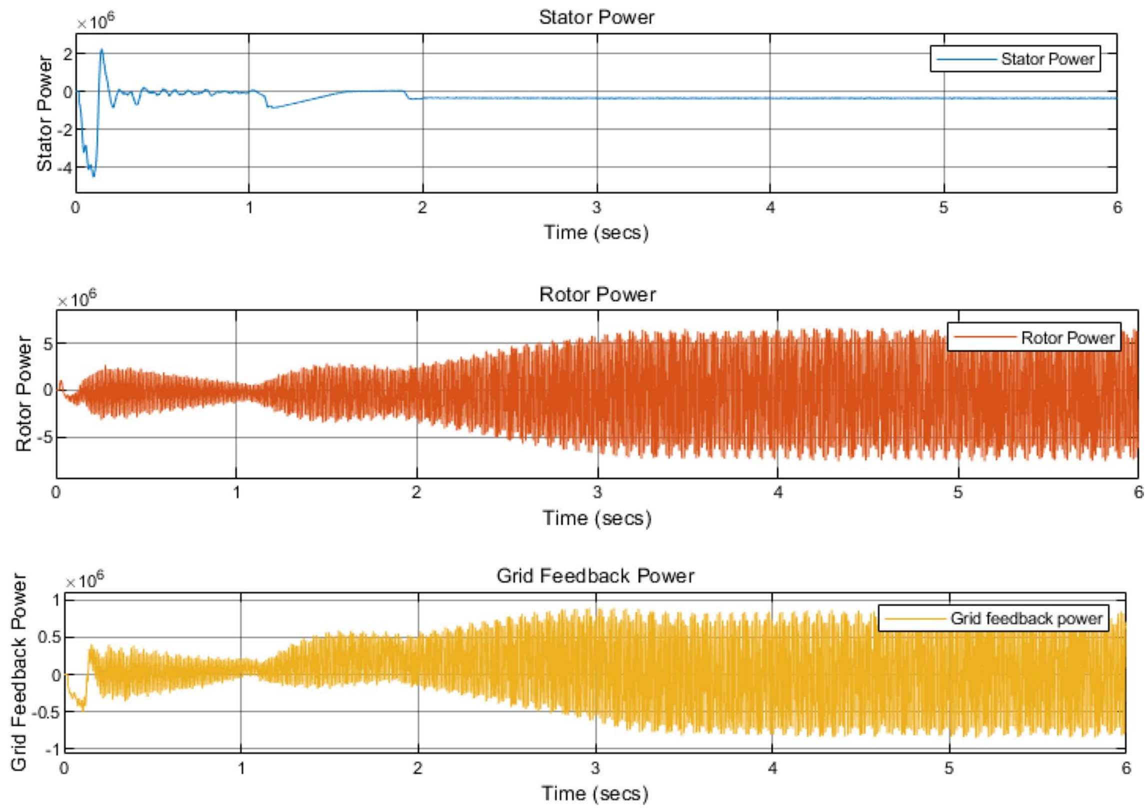

Fig. 28 Stator power, rotor power and grid feedback power of the hybrid system at 8m/s using TSR MPPT algorithm running at synchronous speeds.

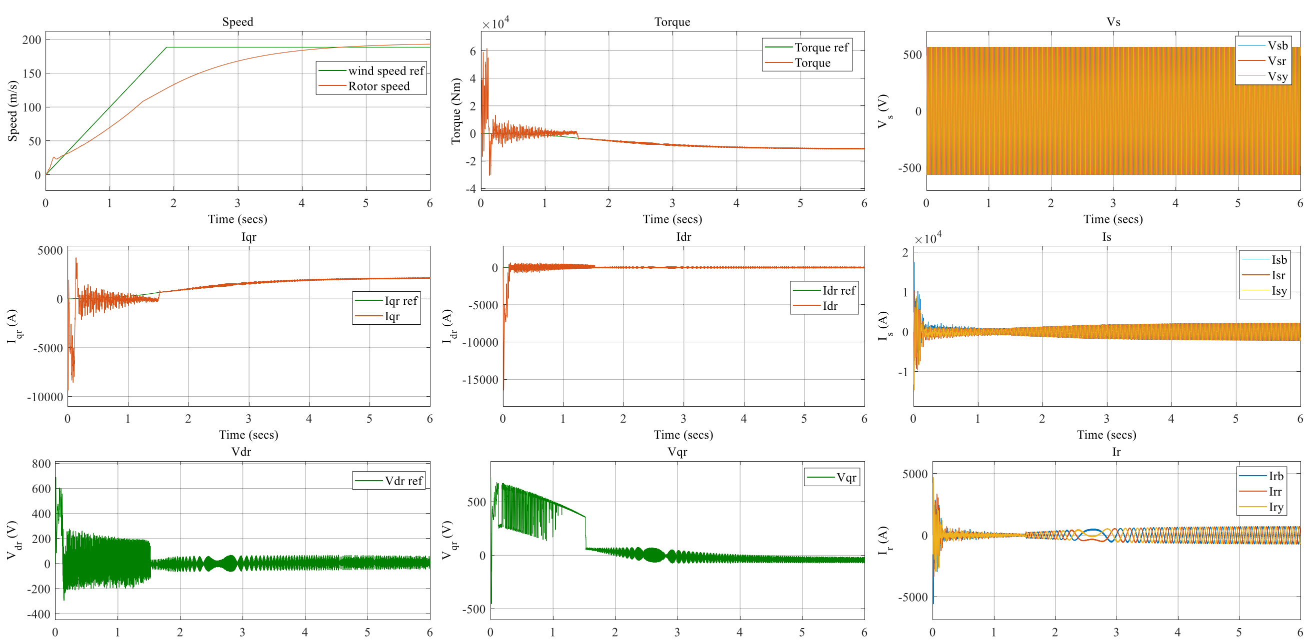

Fig. 29 Graphs of all parameters like (wind speed, torque, d-q voltages and currents, stator voltage, stator current and rotor current variation) with respect to time under OT algorithm running at synchronous speeds

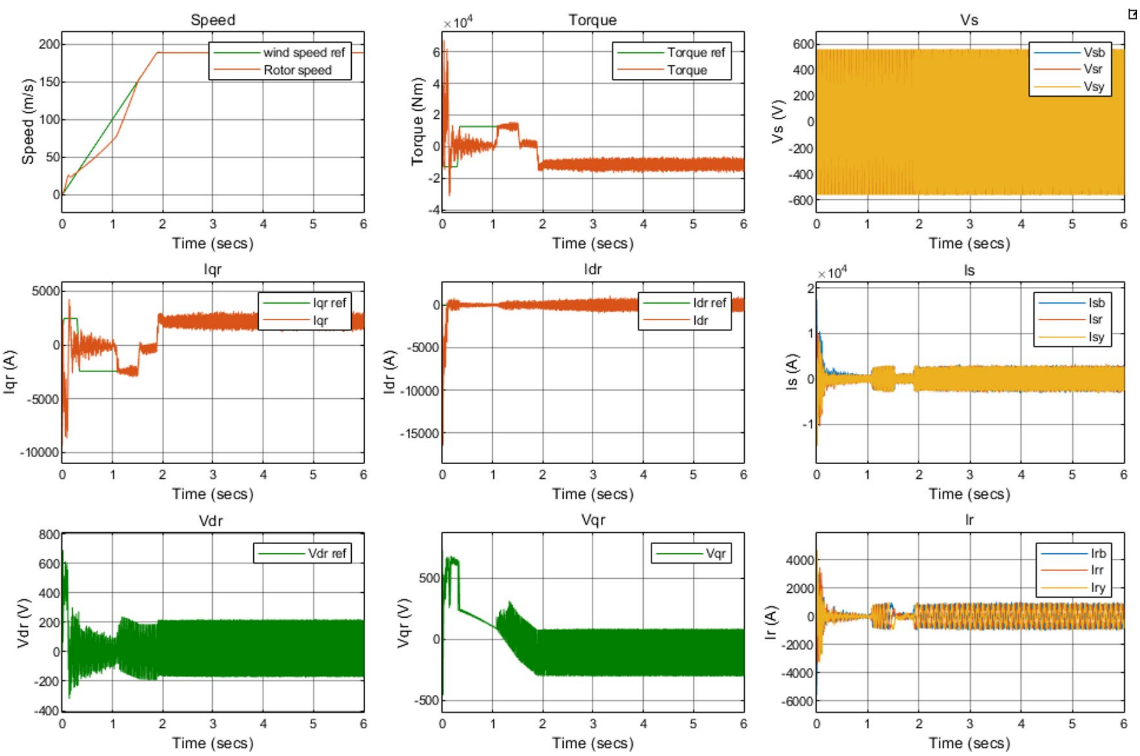

Fig. 30 Graphs of all parameters like (wind speed, torque, d-q voltages and currents, stator voltage, stator current and rotor current variation) with respect to time under TSR algorithm running at synchronous speeds.

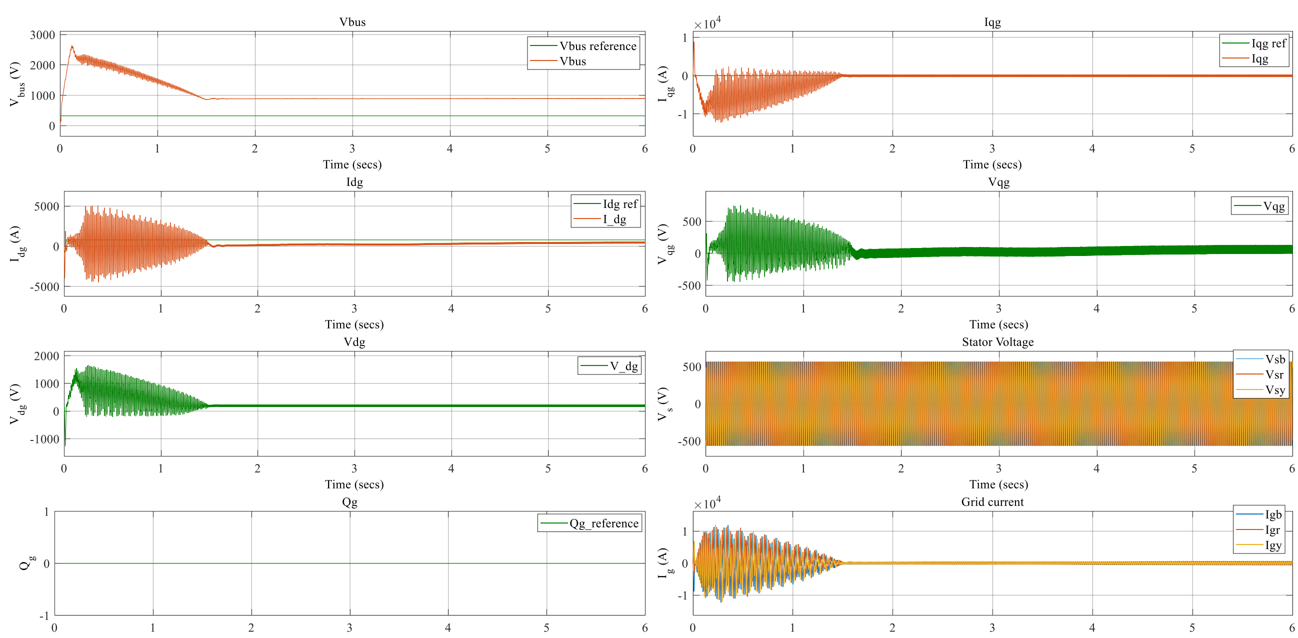

Fig. 31 The grid-side controller waveforms, which include DC bus voltage, d-q axis voltage and current and grid current using optimal torque algorithm running at synchronous speeds.

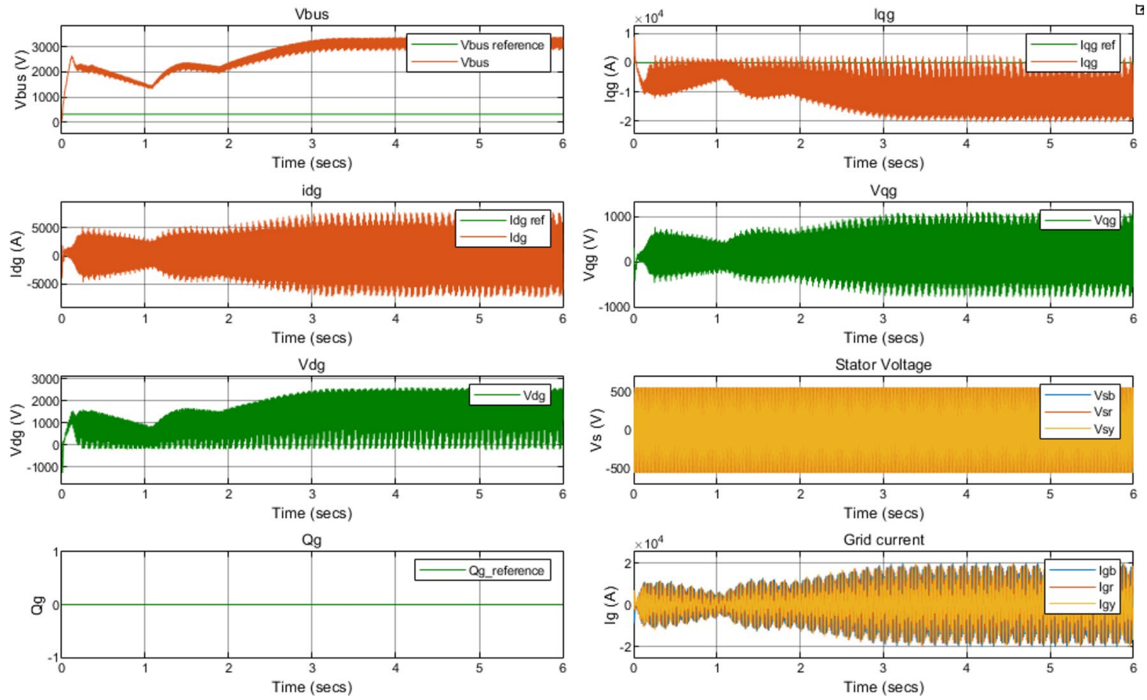

Fig. 32 The grid-side controller waveforms, which include DC bus voltage, d-q axis voltage and current and grid current using TSR algorithm running at synchronous speeds.

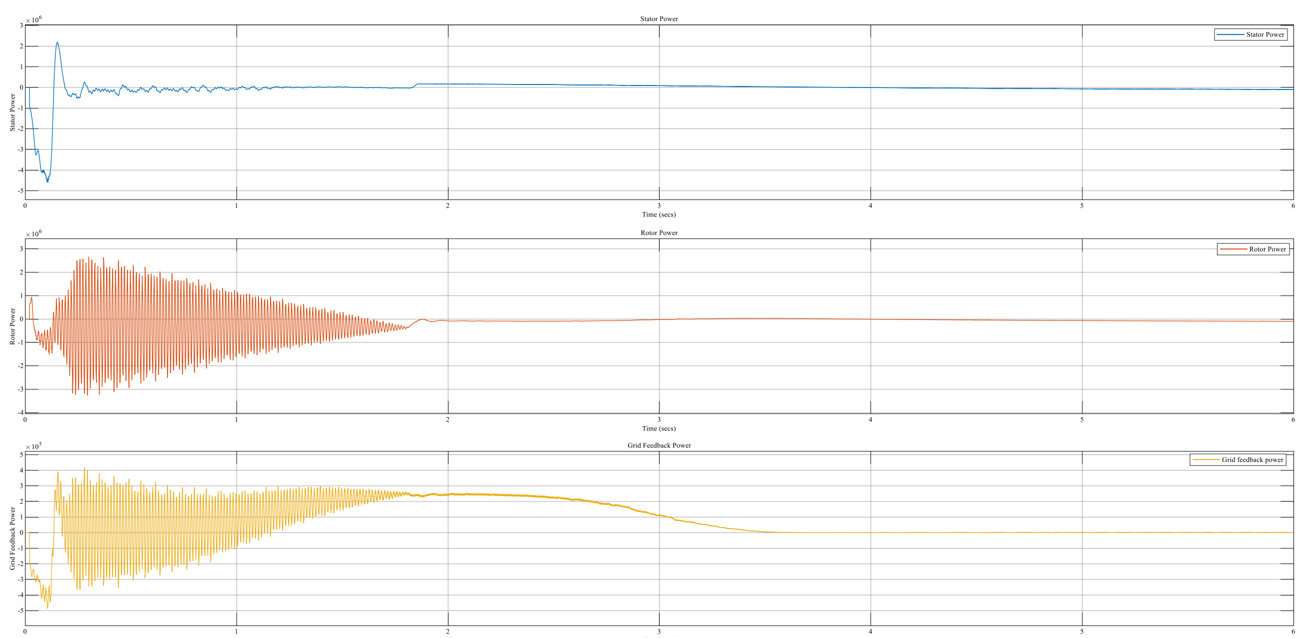

Fig. 33 Stator and rotor power graphs of hybrid system at super synchronous speed using OT algorithm.

for the system running at super synchronous mode, the bus voltage is large compared to the expected bus voltage. To compensate for the large bus voltage, the d-q axes voltage and currents increases, thereby increasing the grid current induced in the grid. This indicates that large reactive power is drawn from the grid, which hampers the performance of the system. On the other hand, the OT method has constant DC link voltage thus produce steady

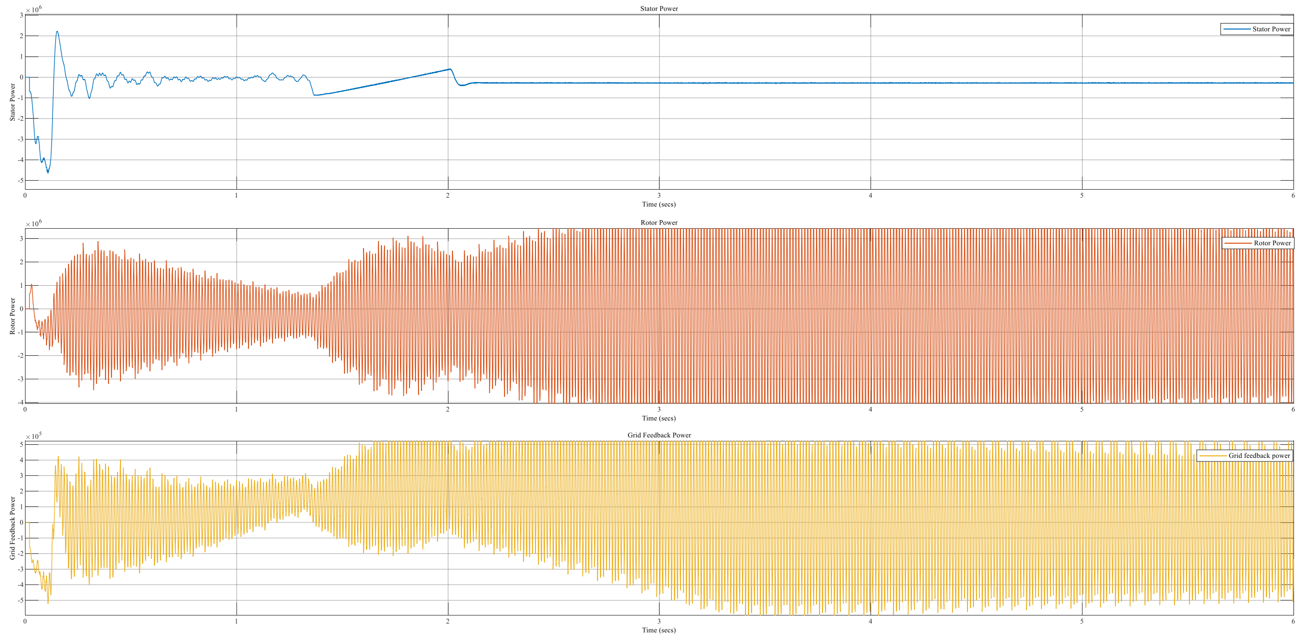

Fig. 34 Stator and rotor power graphs of hybrid system at super synchronous speed using TSR algorithm.

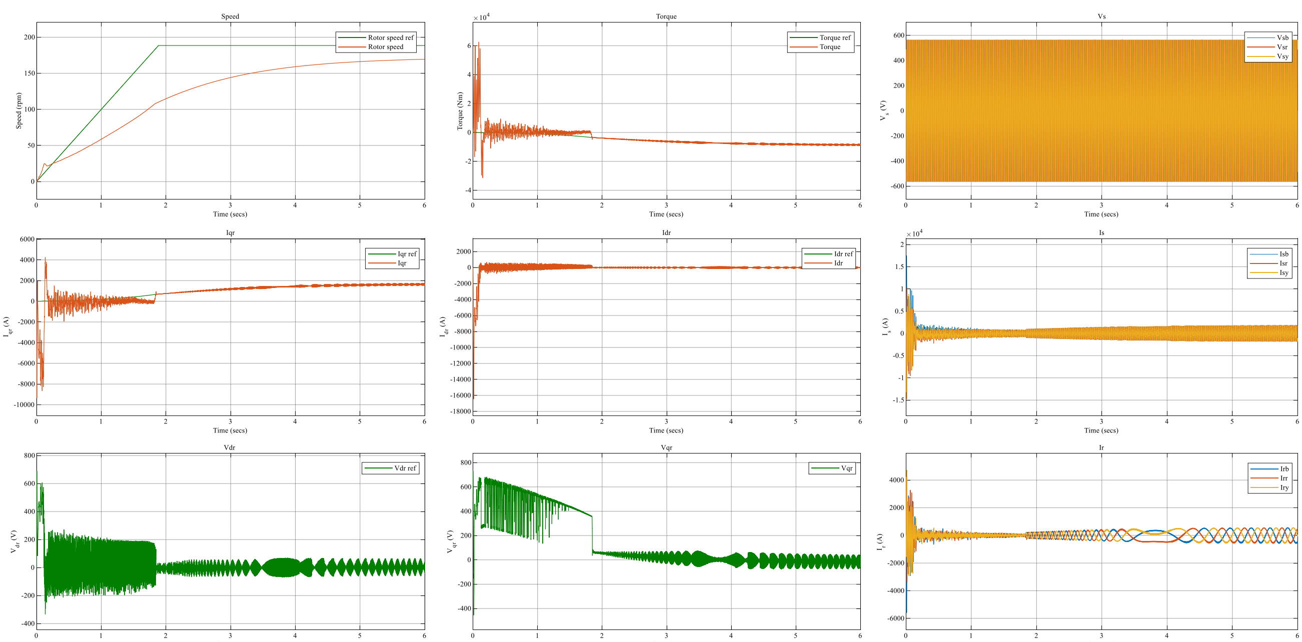

Fig. 35 Rotor side control parameters of hybrid system running at super synchronous speed using OT algorithm.

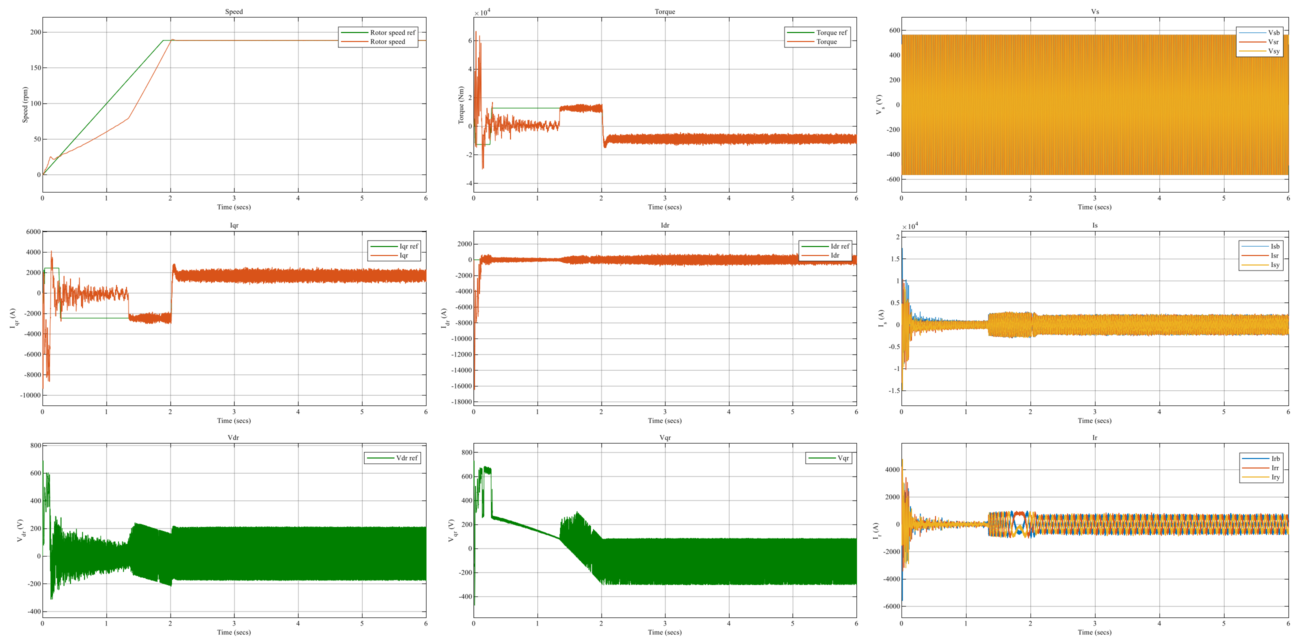

Fig. 36 Rotor side control parameters of hybrid system running at super synchronous speed using TSR algorithm.

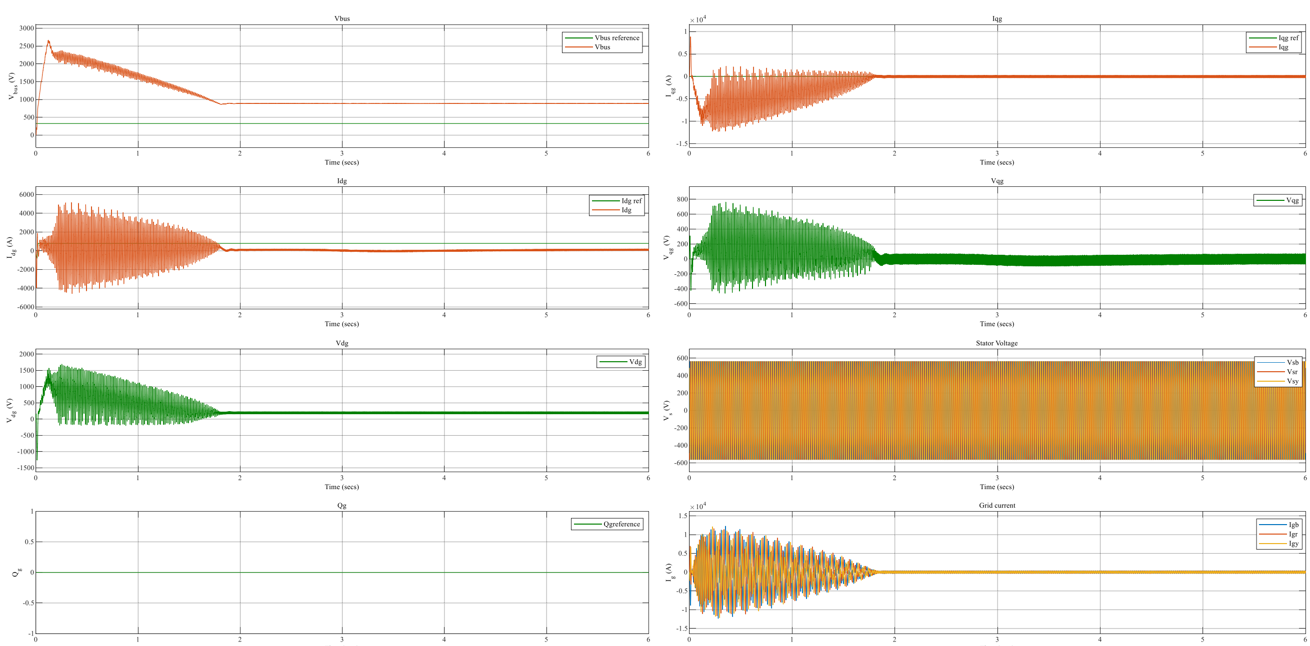

Fig. 37 Grid side control parameters of hybrid system running at super synchronous speed using OT algorithm.

electrical power and feds to the grid. The variation of the bus voltages can be observed at 1.8 sec in the graph.

Hence optimal torque MPPT method has better results compared to the TSR method for all the regions of the wind-speed control characteristics.

Conclusion

The simulation model of the proposed hybrid wind-solar energy system (HWSES) is presented in this paper using

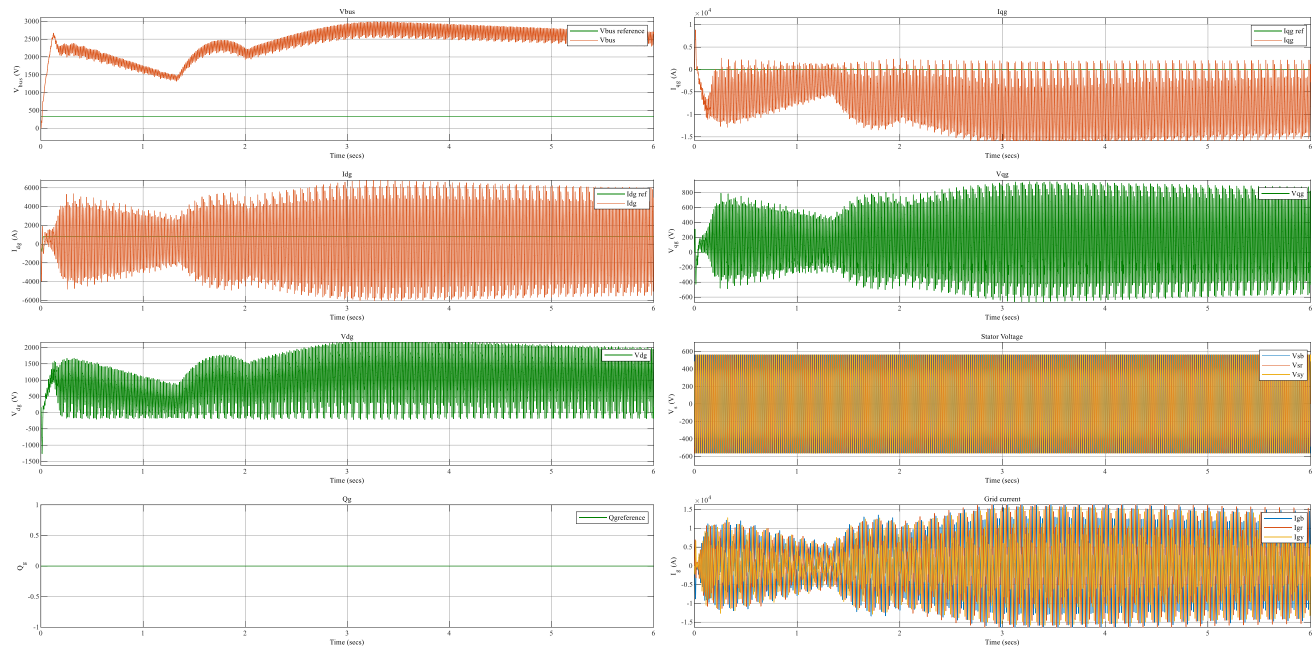

Fig. 38 Grid side control parameters of hybrid system running at super synchronous speed using TSR algorithm.

MATLAB/Simulink environment. This paper addresses the advantage of the solar PV model connected to the dc-link of the back-to-back converter. It also addresses the reduced dependency of the power from the grid, thereby feeding the excess power to the grid. MPPT algorithms also play an important role in increasing the efficiencies of the overall system. Simulation results on a standalone PV system using P&O clearly indicates that the algorithm is better, compared to IC in terms of efficiency. Hence, this algorithm is used in the hybrid wind-solar system model to maximize the power capture from the solar. Wind solar hybrid system is simulated using the MATLAB Simulink model and uses TSR and OT MPPT algorithms to control and maximize the output power. The results show that the optimal torque system has a better dynamic response to the variation of the wind speed when compared to the TSR method. Hence, the optimal torque MPPT method shows better results for the proposed hybrid model. The implemented schemes have the advantage of tracking the optimal power output of the HWSES rapidly and precisely. Additionally, the provided schemes effectively control the power flowing through the HWSES and the utility grid, resulting in a quick transient response and enhanced stability performance and cost-effective approach in stand-alone implementations in remote locations where grid expansion is difficult.

Funding This research received no specific grant from any funding agency in the public, commercial, or not-for-profit sectors

Declarations

Conflicts of interest The author(s) declared no potential conflicts of interest with respect to the research, authorship and/or publication of this article.

Reference

1. Rajanna, S., Saini, R.P.: Modeling of integrated renewable energy system for electrification of a remote area in India. Renewable Energy. 90, 175–187 (2016)
2. Ciupăgeanu, Alexandra, Lăzăroiu, Gheorghe, Barelli, Linda: Wind energy integration: Variability analysis and power system impact assessment. Energy. **185**, 1183–1196 (2019)
3. Dana-Alexandra Ciupageanu., Linda Barelli., Gheorghe Lazaroiu.: Real-time stochastic power management strategies in hybrid renewable energy systems: A review of key applications and perspectives. Electric Power Systems Research. 187, 106497 (2020)
4. Mahesh, Aeidapu: Kanwarjit Singh Sandhu,: Hybrid wind/photovoltaic energy system developments: Critical review and findings. Renewable and Sustainable Energy Reviews **52**, 1135–1147 (2015)
5. Arjun Kumar, G. B, Shivashankar.: Efficient solar integrated doubly fed induction generator for wind energy harnessing. In: Recent Advances in Electrical & Electronic Engineering (Formerly Recent Patents on Electrical & Electronic Engineering) **13**(5), 723–735 (2020)
6. Arjun Kumar, G. B., Shivashankar., Keshavamurthy.: Design and control of solar-Wind Integrated conversion system with DFIG for maximum power point tracking. In: 2020 International conference on recent trends on electronics, information, communication & technology (RTEICT), pp. 292–298 (2020).

7. Hemeida, A. M., El-Ahmar, M. H., El-Sayed, A. M., Hany., Hasanien, M., Salem Alkhalaf, M. F. C., Esmail, Senjyu, T.: Optimum design of hybrid wind/PV energy system for remote area. Ain Shams Eng J **11**(1), 11–23 (2020).
8. Manwell, J. F.: Hybrid Energy Systems. Editor(s): Cutler J. Cleveland. Encyclopedia of Energy. pp. 215–229. Elsevier, Massachusetts (2004)
9. International Renewable Energy Agency. https://www.irena.org/publications/2020/Mar/Renewable-Capacity-Statistics (2021). Accessed 1 Jan 2021
10. Global Wind Energy Council, Online Available. http://www.gwec.net/global-figures/graphs (2021). Accessed 5 Jan 2021
11. Anik Goswami., Paromita Sadhu., Pradip Kumar Sadhu.: Development of a Grid Connected Solar-Wind Hybrid System With Reduction in Levelized Tariff for a Remote Island in India. J. Sol. Energy Eng. vol. 142, no. 4, pp. 044501 (2020)
12. Ministry of New and Renewable Energy. hhttps://mnre.gov.in/img/documents/uploads/2775b59919174bb · 7aeb00bb1d5cd269c.pdf (2021). Accessed 5 Jan 2021
13. Ghulam Sarwar Kaloi: Jie Wang, Mazhar Hussain Baloch,: Active and reactive power control of the doubly fed induction generator based on wind energy conversion system. Energy Reports **2**, 194–200 (2016)
14. Shafiqur Rehman.: Hybrid power systems – Sizes, efficiencies and economics. Energy Exploration & Exploitation 39(1), 3–43 (2020)
15. Bhandari, B., Poudel, S. R., Lee, KT. et al.: Mathematical modeling of hybrid renewable energy system: A review on small hydro-solar-wind power generation. Int. J. of Precis. Eng. and Manuf.-Green Tech1, 157–173 (2014)
16. Amevi Acakpovi, Patrick Adjei, Nnamdi Nwulu, Nana Yaw Asabere.: Optimal Hybrid Renewable Energy System: A Comparative Study of Wind/Hydrogen/Fuel-Cell and Wind/Battery Storage. J Elect Comput Eng **1756503**, 1–15 (2020)
17. Zhu, Rui, Zhao, An.-lei, Wang, Guang-chao, Xia, Xin, Yang, Yaopan: An Energy Storage Performance Improvement Model for Grid-Connected Wind-Solar Hybrid Energy Storage System. Computational Intelligence and Neuroscience **8887227**, 1–10 (2020)
18. Hossam, H.H., Mousa., Abdel-Raheem Youssef., Essam, E.M., Mohamed.: Hybrid and adaptive sectors P&O MPPT algorithm based wind generation system. Renew Energy **145**, 1412–1429 (2020)
19. İrfan Yazıcı., Ersagun Kürşat Yaylacı.: Improving efficiency of the tip speed ratio-MPPT method for wind energy systems by using an integral sliding mode voltage regulator. J. Energy Resour. Technol. **140**(5), 051203–051209 (2018)
20. Song, D., Yang, J., Su, M., Liu, A., Liu, Y., Joo, Y.H.: A Comparison Study between Two MPPT Control Methods for a Large Variable-Speed Wind Turbine under Different Wind Speed Characteristics. Energies **10**(5), 61 (2017)
21. Bourdoulis., Michael, K., and Antonio, T., Alexandridis.: PI control design and passivity/stability analysis for DFIG wind systems under vector control constraints. Software Engineering / 781 Control Applications. https://doi.org/10.2316/P.2012.781-035 (2012)
22. Soliman, M. A., Hasanien, H. M., Alkuhayli, A.: Marine predators algorithm for parameters identification of triple-diode photovoltaic models. IEEE **8**, 1–15 (2020).
23. Karad, S., Thakur, R.: Recent trends of control strategies for doubly fed induction generator based wind turbine systems: A comparative review. Arch Computat Methods Eng **28**, 15–29 (2021)
24. Ali Omar Baba., Guangyu Liu., Xiaohui Chen.: Classification and Evaluation Review of Maximum Power Point Tracking Methods. Sustainable Futures. 2, 100020 (2020)
25. Kamran, Muhammad, et al.: Implementation of improved Perturb & Observe MPPT technique with confined search space for standalone photovoltaic system. Journal of King Saud University - Engineering Sciences **32**(7), 432–441 (2020)
26. Pakkiraiah, B., Durga Sukumar, G.: Research Survey on Various MPPT Performance Issues to Improve the Solar PV System Efficiency. Journal of Solar Energy 2016(8012432), 1–20 (2016)

Publisher's Note Springer Nature remains neutral with regard to jurisdictional claims in published maps and institutional affiliations.